pharmaceuticals

MDPI

Article

Jiebai-Qingfei San Protects Against Lipopolysaccharide-Induced Acute Lung Injury by Modulating Inflammation, Oxidative Stress, and Macrophage-Associated Phenotypes

Xiangwen Deng [1,2], Jin He [3], Lin Yu [1,2], Yaming Yu [1,2], Kexin Fang [1,2], Yang Yang [1,2,*] and Deyun Wang [1,2,*]

[1] Institute of Traditional Chinese Veterinary Medicine, College of Veterinary Medicine, Nanjing Agricultural University, Nanjing 210095, China; dengxiangwen@stu.njau.edu.cn (X.D.); yulin@stu.njau.edu.cn (L.Y.); hnyuym@163.com (Y.Y.); kxfang@njau.edu.cn (K.F.)
[2] MOE Joint International Research Laboratory of Animal Health and Food Safety, College of Veterinary Medicine, Nanjing Agricultural University, Nanjing 210095, China
[3] Key Laboratory of Traditional Chinese Veterinary Medicine and Animal Health in Fujian Province, College of Animal Sciences, Fujian Agriculture and Forestry University, Fuzhou 350002, China; xiaoxiaofengqiu@163.com
* Correspondence: yangyang@njau.edu.cn (Y.Y.); dywang@njau.edu.cn (D.W.)

Abstract

Background: Jiebai-Qingfei San (JBQFS) is a seven-herb traditional Chinese veterinary formulation developed for respiratory disorders. However, its pharmacological effects against acute pulmonary inflammation and the associated molecular responses remain unclear. This study examined the protective activity of JBQFS in LPS-induced acute lung injury (ALI) and characterized the biological responses associated with treatment. **Methods**: The chemical profile of JBQFS was characterized by ultra-high-performance liquid chromatography coupled with high-resolution tandem mass spectrometry (UHPLC-HRMS/MS), and two representative marker compounds were quantified by high-performance liquid chromatography (HPLC). Lung transcriptomic analysis followed by qRT-PCR validation was performed to identify inflammation-related transcriptional responses. The effects of JBQFS were further examined in the murine alveolar macrophage cell line MH-S following LPS stimulation. **Results**: JBQFS pretreatment ameliorated LPS-induced alterations in respiratory parameters and attenuated histopathological injury, reduced inflammatory cytokine levels, and improved oxidative stress-related parameters. It also modulated macrophage-associated markers in lung tissue. Transcriptomic and qRT-PCR analyses showed that JBQFS administration was associated with changes in inflammation-related transcriptional responses, including genes related to TLR4/MyD88/NF-κB signaling. In MH-S cells, JBQFS reduced inflammatory mediator production and intracellular ROS and Ca^{2+} levels, preserved mitochondrial membrane potential, and modulated CD80, CD86, and CD206 expression. **Conclusions**: Pretreatment with JBQFS protected against LPS-induced ALI and was associated with reduced inflammation and oxidative stress, as well as modulation of macrophage-associated inflammatory phenotypes. These findings support further investigation of JBQFS for inflammatory respiratory disorders.

Keywords: acute lung injury; Jiebai-Qingfei San; lipopolysaccharide; macrophage; oxidative stress; traditional Chinese medicine

Check for updates

Academic Editors: Jorge P. Machado, Maria Helena Chéu and Maria Begoña Criado

Received: 10 October 2026
Revised: 5 November 2026
Accepted: 13 November 2026
Published: 18 November 2026

Copyright: © 2026 by the authors. Licensee MDPI, Basel, Switzerland. This article is an open access article distributed under the terms and conditions of the Creative Commons Attribution (CC BY) license.

1. Introduction

Acute lung injury (ALI) is characterized by increased pulmonary vascular permeability, pulmonary edema, impaired gas exchange, and excessive inflammatory responses [1,2].

ALI can result from a variety of direct and indirect insults, including sepsis, pneumonia, aspiration, and inhalation injury, and severe cases may progress to acute respiratory distress syndrome (ARDS) [3]. During the pathogenesis of ALI, massive infiltration of neutrophils and macrophages into the lungs leads to excessive cytokine production and hyperinflammatory responses, which exacerbate lung tissue injury [4,5]. This process also compromises the pulmonary epithelial barrier, promoting pulmonary edema and increasing vascular permeability, further upregulating multiple pro-inflammatory factors [6,7]. Pulmonary endothelial inflammation also contributes to ALI, and SIRT6 activation has been shown to attenuate LPS-induced VCAM1 expression and monocyte adhesion in human lung microvascular endothelial cells [8]. Thus, restraining systemic hyperinflammation and reducing local pulmonary cytokine levels are crucial for therapeutic intervention. Although available strategies include pharmacological agents and mechanical ventilation, their long-term use is constrained by adverse effects and limited efficacy, and ventilation itself may cause fibrotic complications [9]. Therefore, new strategies to alleviate pulmonary inflammation, oxidative stress, and tissue injury are still needed.

Traditional Chinese Medicine (TCM) has a longstanding clinical track record in managing respiratory disorders and a well-established history of anti-inflammatory use [10]. In experimental lung injury, TCM interventions have been shown to alleviate pulmonary inflammation and regulate inflammatory and oxidative responses [11,12]. Herbal medicines and multi-component formulations may exert anti-inflammatory, antioxidant, and immunoregulatory effects through multiple biological targets [13]. Accumulating evidence indicates that Xuanfei Baidu Decoction ameliorates ALI by downregulating pro-inflammatory mediators and reducing macrophage/neutrophil infiltration via the PD-1/IL-17A and NF-κB pathways [14,15]. Shiwei Qingwen Decoction has shown protective activity against ALI, with reported effects on TLR4/NF-κB signaling and NLRP3 inflammasome activation [16]. Furthermore, other herbal formulas—including Guben Qingfei Decoction, Sanzi Yangqin Decoction, and Sanhuang Xiexin Decoction—have also shown beneficial effects against ALI [5,17,18]. Although previous studies have demonstrated the protective effects of various herbal formulations against experimental ALI, their findings cannot be directly extrapolated to JBQFS, which differs in herbal composition and intended veterinary application.

Jiebai-Qingfei San (JBQFS) is a seven-herb formulation comprising Jiegeng, Baibu, Cheqiancao, Dafupi, Gancao, Huzhang, and Zhimu. The formulation was developed for veterinary use and has been granted a Chinese invention patent for its application in the prevention and treatment of bovine respiratory diseases (ZL202311347908.5; CN117138004B). Several constituent herbs have reported pharmacological activities relevant to respiratory disorders. Platycodon grandiflorus has traditionally been used to treat respiratory conditions [19]. Pharmacological studies have demonstrated that *P. grandiflorus* modulates immune responses and cytokine production and suppresses mucus hypersecretion [19–21]. *Stemona japonica* (Baibu) is traditionally used for respiratory ailments, particularly cough, and its principal alkaloids exhibit antitussive, anti-fibrotic, and anti-inflammatory activities, with protective effects reported in experimental models of asthma and Gram-negative bacterial-induced ALI [22,23]. *Glycyrrhiza uralensis* (licorice) has traditionally been used for respiratory conditions such as cough, bronchitis, and pneumonia [24], while its bioactive flavonoids have been reported to attenuate LPS-induced ALI through modulation of cGAS-STING and TLR4/MyD88/NF-κB-related signaling pathways [25,26]. *Anemarrhena asphodeloides* Bunge (Zhimu), traditionally indicated for febrile conditions associated with pulmonary heat and dry cough [27], contains steroidal saponins and polysaccharides with reported anti-inflammatory activities. *Steroidal saponins* from A. asphodeloides, including Timosaponin A-III, have been reported to inhibit inflammatory responses in experimental

models of lung inflammation [28,29]. However, the protective effects of the complete JBQFS formulation against ALI and the associated biological responses remain unclear.

In the present study, we evaluated JBQFS in an LPS-induced ALI mouse model by assessing respiratory parameters, lung injury, inflammatory and oxidative responses, and macrophage-associated phenotypic markers. Lung transcriptomic analysis and experiments in LPS-stimulated MH-S cells were further performed to investigate the molecular and cellular responses associated with JBQFS treatment.

2. Results

2.1. Chemical Characterization of JBQFS by UHPLC-HRMS/MS

Non-targeted UHPLC-HRMS/MS analysis was performed to characterize the chemical profile of JBQFS. Representative total ion chromatograms (TICs) acquired in negative- and positive-ion modes are presented in Figure 1. A total of 715 and 260 chemical features were assigned candidate annotations in positive- and negative-ion modes, respectively. Ten representative features, including candidates corresponding to mangiferin, polydatin, liquiritin, isoliquiritin, and glycyrrhizic acid, are summarized in Table 1.

Additionally, HPLC analysis was performed to quantify glycyrrhizic acid and polydatin in three independent batches of JBQFS. Their respective contents were 3.070 ± 0.057 and 2.403 ± 0.012 mg/g (mean ± SD; Supplementary Method S1, Table S1, and Figures S1 and S2).

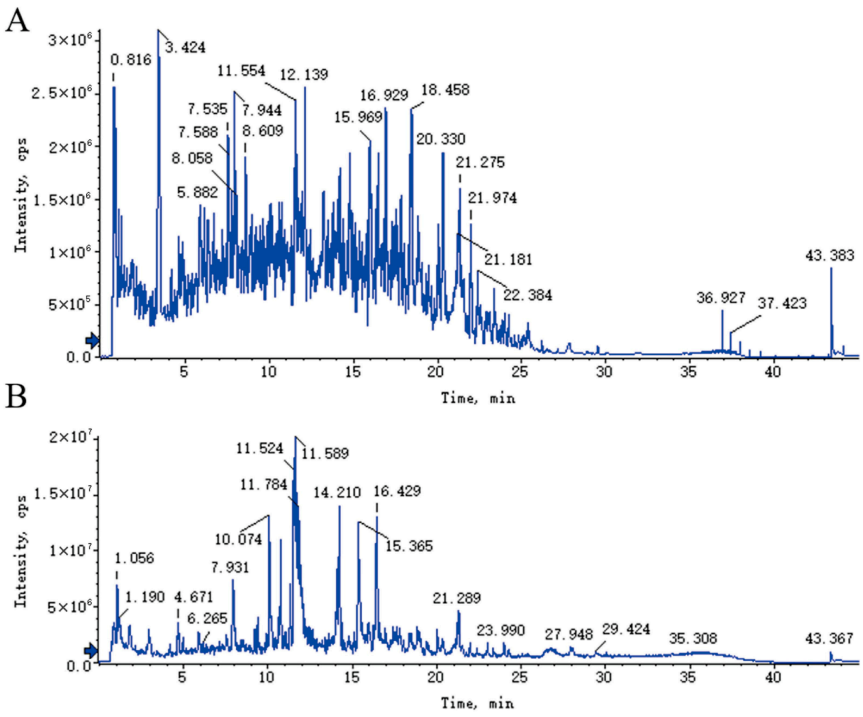


Figure 1. Representative total ion chromatograms (TICs) of JBQFS obtained by UHPLC-HRMS/MS. (**A**) Negative-ion mode. (**B**) Positive-ion mode.

Table 1. Representative UHPLC-HRMS/MS features and tentative database-derived annotations of JBQFS.

Name	RT (min)	Observed *m*/*z*	Adduct	Calculated *m*/*z*	Formula	Mass Error (ppm)
Arecoline	0.917	156.10133	$[M + H]^+$	156.10193	$C_8H_{13}NO_2$	−3.68
Mangiferin	6.155	423.09286	$[M + H]^+$	423.09221	$C_{19}H_{18}O_{11}$	1.59

Table 1. *Cont.*

Name	RT (min)	Observed *m*/*z*	Adduct	Calculated *m*/*z*	Formula	Mass Error (ppm)
Polydatin (Piceid)	6.646	391.13996	$[M + H]^+$	391.13877	$C_{20}H_{22}O_8$	3.11
Chrysophanol 8-O-β-D-glucoside	7.432	417.11893	$[M + H]^+$	417.11803	$C_{21}H_{20}O_9$	2.21
Luteolin 7-O-β-D-glucoside	8.126	449.10909	$[M + H]^+$	449.10786	$C_{21}H_{20}O_{11}$	2.79
Liquiritin	7.816	417.11883	$[M - H]^-$	417.11904	$C_{21}H_{22}O_9$	−0.66
Isoliquiritin	7.932	417.11925	$[M - H]^-$	417.11908	$C_{21}H_{22}O_9$	0.35
Liquiritin apioside	8.037	549.16103	$[M - H]^-$	549.16134	$C_{26}H_{30}O_{13}$	−0.61
Glycyrrhizic acid	17.265	821.39609	$[M - H]^-$	821.39651	$C_{42}H_{62}O_{16}$	−0.51
Torachrysone 8-glucoside	11.992	407.13559	$[M - H]^-$	407.13473	$C_{20}H_{24}O_9$	2.05

Note: RT, retention time; MSI, Metabolomics Standards Initiative. Compound names represent tentative database-derived structural candidates. In the absence of verifiable compound-specific MS/MS spectral matches, all listed features were conservatively classified as MSI level 4. Structural and positional isomers could not be reliably distinguished. Calculated *m*/*z* values were obtained from the molecular formulas and corresponding adduct ions.

2.2. JBQFS Ameliorates Respiratory Alterations and Histopathological Injury in ALI Mice

The effects of JBQFS pretreatment were first assessed in mice with LPS-induced ALI (Figure 2A). LPS challenge increased the lung wet/dry ratio relative to the CON group ($p < 0.01$), whereas the ratio was reduced in the JBQFS-M and JBQFS-H groups ($p < 0.01$; Figure 2B).

Whole-body plethysmography (WBP) was performed to evaluate respiratory parameters, including tidal volume (TV), minute ventilation (MV), peak expiratory flow (PEF), enhanced pause (Penh), and total breath duration (TB) (Figure 2C–G). The effects of JBQFS on WBP-derived respiratory parameters varied across measurements and doses, with TV, MV, and TB showing no consistent dose-dependent pattern (Figure 2C–G).

H&E staining revealed acute LPS-associated pathological changes in lung architecture, including alveolar septal thickening, inflammatory cell infiltration, and disruption of alveolar structures. These changes were less pronounced in the JBQFS-treated groups (Figure 2H). Consistent with the histological observations, semiquantitative assessment showed higher lung injury scores in the LPS group, whereas lower scores were observed in the JBQFS-L and JBQFS-H groups, with an intermediate score in the JBQFS-M group (Figure 2I). Together with the W/D ratio and respiratory parameters, the histopathological findings support the protective effects of JBQFS against LPS-induced acute lung injury.

2.3. JBQFS Attenuates Inflammatory Responses

Pulmonary inflammatory responses were further evaluated by assessing IL-6, TNF-α, and IL-1β at both the transcriptional and protein levels. Their mRNA expression in lung tissues was quantified by qRT-PCR (Figure 3A–C), while cytokine concentrations in BALF and serum were determined by ELISA. Consistent with the aforementioned results, LPS challenge significantly upregulated the mRNA expression of pro-inflammatory cytokines (IL-6, TNF-α and IL-1β) in lung tissues, and markedly increased their protein levels in both BALF and serum ($p < 0.01$; Figure 3D–I). However, pretreatment with JBQFS at low, medium, and high doses attenuated LPS-induced elevations in pulmonary inflammatory cytokine levels (Figure 3A–I). Notably, high-dose JBQFS showed the strongest inhibitory effect on IL-6, TNF-α, and IL-1β expression, as evidenced by reduced cytokine mRNA levels in lung tissues and decreased cytokine protein levels in BALF and serum, especially in serum ($p < 0.01$). These data indicate that JBQFS attenuates both local pulmonary and systemic inflammation induced by LPS.

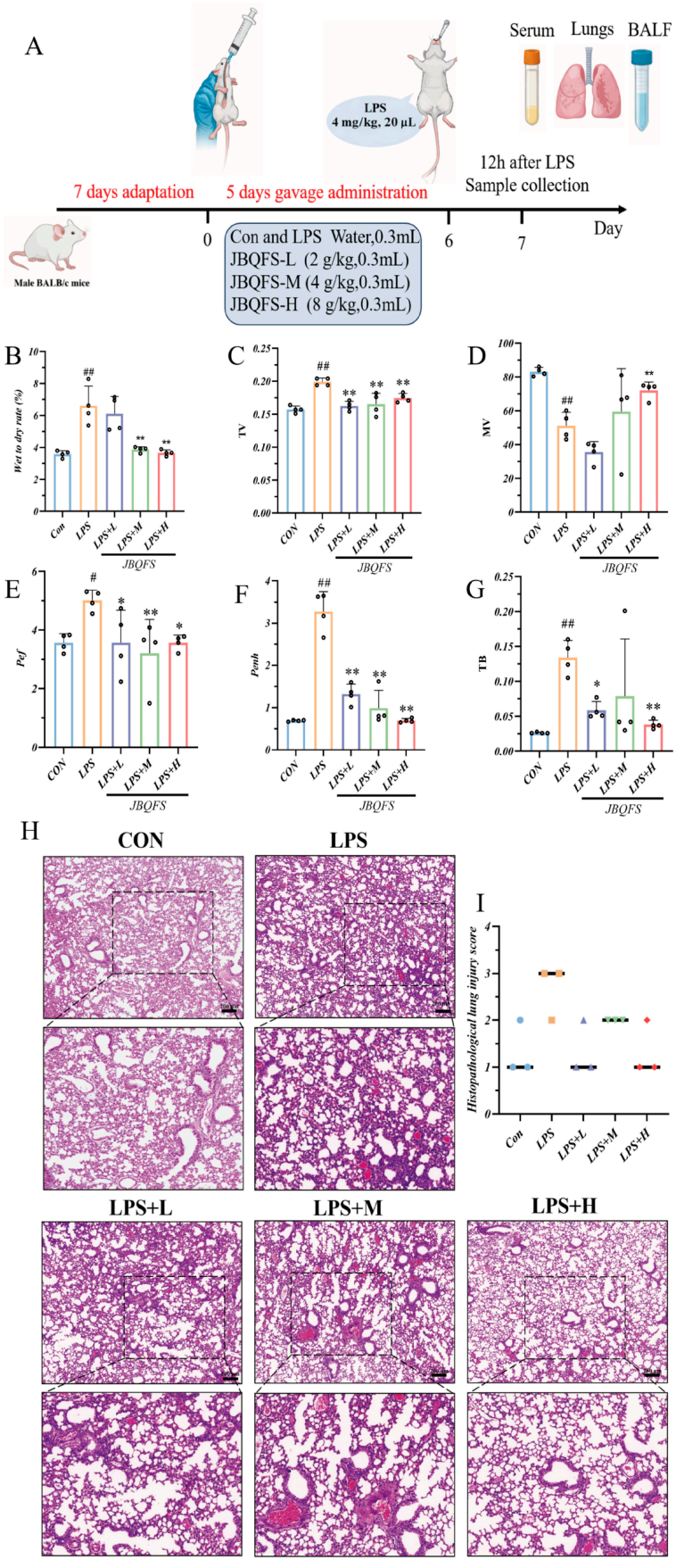


Figure 2. JBQFS ameliorated LPS-induced alterations in respiratory parameters and histopathological injury in mice. (**A**) Schematic diagram of the animal experimental design. (**B**) Lung wet-to-dry weight ratio. (**C**–**G**) Respiratory parameters measured by whole-body plethysmography, including

tidal volume (TV), minute ventilation (MV), peak expiratory flow (PEF), enhanced pause (Penh), and total breath duration (TB). (**H**) Representative H&E-stained lung sections from the five experimental groups. Lower panels show magnified views of the indicated regions. (**I**) Semiquantitative histopathological lung injury scores, with higher scores indicating more severe lung injury. $n = 4$ mice per group for W/D and respiratory parameter analyses (**B**–**G**), and $n = 3$ mice per group for histopathological assessment (**H**,**I**). Data in B–G are presented as mean ± SD. Histopathological scores in I are presented as individual animal values with the median and were analyzed using the Kruskal–Wallis test followed by Dunn's multiple-comparison test. # $p < 0.05$ and ## $p < 0.01$ versus the CON group; * $p < 0.05$ and ** $p < 0.01$ versus the LPS group.

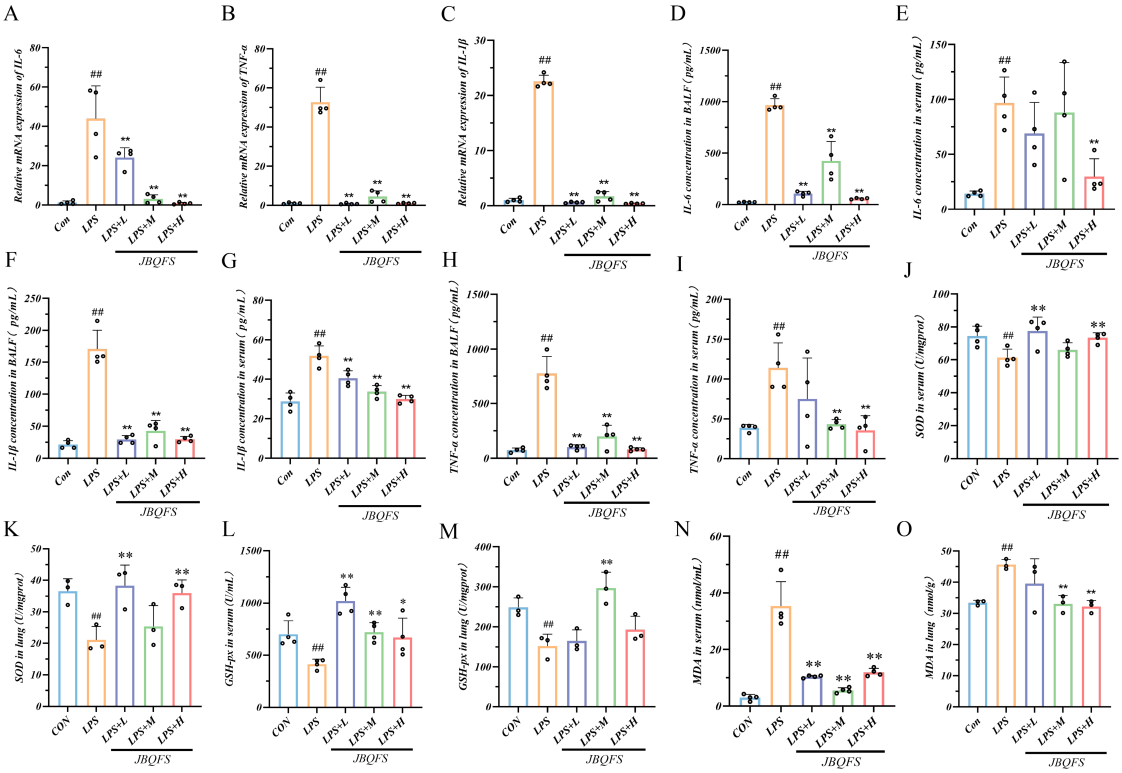


Figure 3. JBQFS suppressed inflammatory cytokine production and improved oxidative stress status in LPS-induced acute lung injury mice. (**A**–**C**) Relative mRNA expression levels of IL-6, TNF-α, and IL-1β in lung tissues. (**D**,**F**,**H**) Concentrations of IL-6, IL-1β, and TNF-α in BALF. (**E**,**G**,**I**) Concentrations of IL-6, IL-1β, and TNF-α in serum. (**J**,**L**,**N**) SOD activity, GSH-Px activity, and MDA levels in serum. (**K**,**M**,**O**) SOD activity, GSH-Px activity, and MDA levels in lung tissues. Samples were collected 12 h after LPS challenge. $n = 4$ mice per group for inflammatory cytokine analyses and serum oxidative-stress measurements; $n = 3$ mice per group for lung-tissue SOD, GSH-Px, and MDA measurements. Data are presented as mean ± SD. ## $p < 0.01$ versus the CON group; * $p < 0.05$ and ** $p < 0.01$ versus the LPS group.

2.4. JBQFS Ameliorates Oxidative Stress in ALI Mice

Oxidative stress was further evaluated by measuring SOD and GSH-Px activities and MDA levels in serum and lung tissues. As presented in Figure 3J–O, compared with the CON group, the LPS group exhibited significantly decreased serum SOD and GSH-Px activities, accompanied by a marked increase in MDA levels ($p < 0.01$). Pretreatment with JBQFS effectively attenuated the reductions in SOD and GSH-Px activities and also lowered serum MDA levels. Consistent with these findings, LPS challenge resulted in elevated MDA concentrations and decreased SOD and GSH-Px activities in lung tissues ($p < 0.05$). In contrast, JBQFS treatment lowered MDA levels and increased SOD and GSH-Px activities in lung tissues compared with the LPS group ($p < 0.01$).

2.5. JBQFS Modulates Macrophage-Associated Inflammatory Markers in Lung Tissue

Macrophages are important regulators of innate immune and inflammatory responses to tissue injury and infection [30]. Depending on the microenvironmental stimuli, macrophages exhibit diverse functional phenotypes [31]. To investigate the regulatory effects of JBQFS on macrophage-associated phenotypic markers in lung tissue, immunofluorescence staining was performed to assess macrophage-associated M1- and M2-related markers. Figure 4 shows that LPS challenge increased the fluorescence signals of F4/80 and the pro-inflammatory macrophage-associated marker CD86 in lung tissues ($p < 0.01$). Compared with the CON group, the LPS group exhibited decreased fluorescence intensity of the anti-inflammatory macrophage-associated marker CD206 and a reduced CD206/F4/80 ratio ($p < 0.01$), suggesting an inflammatory macrophage-associated phenotype in the LPS group. However, JBQFS intervention significantly reduced CD86 fluorescence intensity, markedly upregulated $CD206^+$ cell numbers, decreased the CD86/F4/80 ratio, and increased the CD206/F4/80 ratio in a dose-dependent manner ($p < 0.01$). These findings suggest that JBQFS modulates macrophage-associated inflammatory marker profiles in lung tissue, as reflected by changes in CD86- and CD206-associated signals during acute lung injury. Furthermore, statistical analysis of the CD86/CD206 marker ratio showed that LPS stimulation was associated with an increased CD86/CD206 ratio ($p < 0.01$). In contrast, JBQFS treatment reduced the CD86/CD206 ratio ($p < 0.01$), further supporting its effects on macrophage-associated inflammatory phenotypes. Overall, the changes in CD86- and CD206-associated signals indicate that macrophage-associated inflammatory phenotypes in lung tissue were modulated by JBQFS during LPS-induced ALI.

2.6. Transcriptomic Analysis Identifies Inflammation-Related Transcriptional Responses Associated with JBQFS Administration

To further investigate the potential molecular basis by which JBQFS alleviates LPS-induced ALI, transcriptomic analysis was performed using lung tissues from the CON, LPS, and JBQFS-H groups. As shown in Figure 5A, principal component analysis revealed clear separation among the three groups, indicating distinct transcriptional profiles after LPS challenge and JBQFS-H administration. Compared with the CON group, the LPS group showed 2789 differentially expressed genes (DEGs), comprising 1716 upregulated and 1073 downregulated genes. The JBQFS-H versus LPS comparison yielded 1788 DEGs, of which 642 were upregulated and 1146 were downregulated (Figure 5B).

KEGG enrichment analysis was then performed to explore the biological pathways associated with these gene expression changes. For the LPS versus CON comparison, KEGG enrichment of the DEGs involved multiple inflammation- and immune-related pathways, including cytokine–cytokine receptor interaction, IL-17 signaling pathway, NF-κB signaling pathway, Toll-like receptor signaling pathway, NOD-like receptor signaling pathway, JAK-STAT signaling pathway, and lipid and atherosclerosis (Figure 5C). In the JBQFS-H versus LPS comparison, enriched KEGG terms included cytokine–cytokine receptor interaction, B cell receptor signaling pathway, JAK-STAT signaling pathway, TNF signaling pathway, and other immune- and inflammation-associated pathways (Figure 5D; Table S2). These results suggest that JBQFS-H may regulate LPS-induced pulmonary inflammatory responses at the transcriptional level.

To further evaluate the expression pattern of inflammation-related genes, a heatmap was generated using representative genes involved in inflammatory and immune responses. LPS challenge markedly upregulated the expression of several inflammatory genes, including IL-1β, IL-6, TNF-α, TLR4, MyD88, Ccl2, Cxcl2, and NF-κB-related genes, whereas JBQFS-H pretreatment partially reversed these LPS-induced alterations (Figure 5E). Consistent with the transcriptomic results, qRT-PCR analysis showed that LPS significantly

increased the mRNA expression levels of IL-6, TNF-α, IL-1β, TLR4, MyD88, and NF-κB-related genes in lung tissues. However, JBQFS-H administration significantly reduced the expression of these genes compared with the LPS group (Figure 5F). Together, these results showed that JBQFS-H administration was associated with reduced expression of inflammatory cytokine genes and altered TLR4/MyD88/NF-κB-related transcriptional responses in LPS-challenged lung tissue. Complete differential gene expression and KEGG enrichment results for both comparisons are provided in Supplementary Data S1.

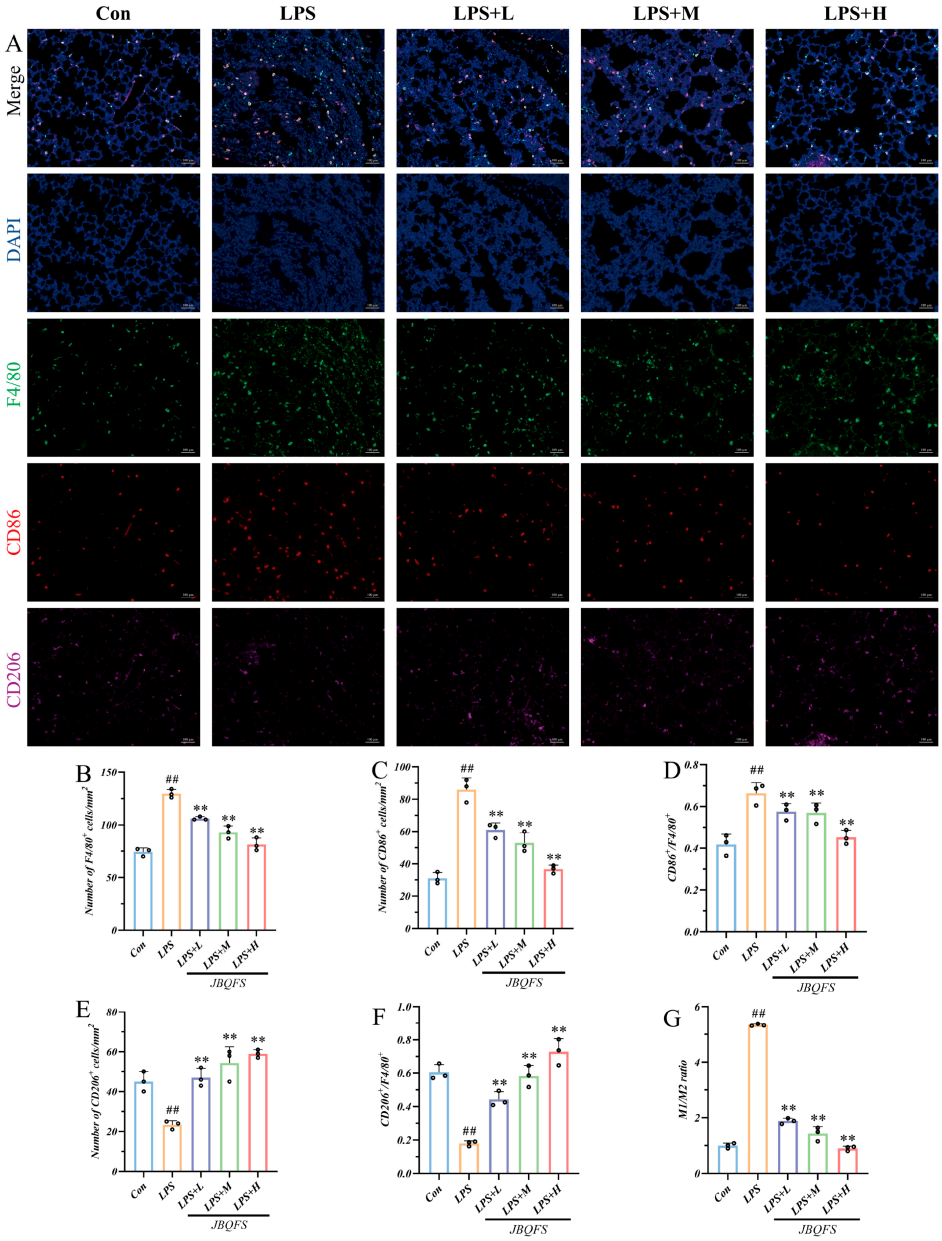


Figure 4. JBQFS modulated macrophage-associated inflammatory phenotypes in lung tissues of LPS-induced acute lung injury mice. (**A**) Representative immunofluorescence images of lung sections stained for F4/80, CD86, CD206, and DAPI. F4/80 was used as a macrophage marker, CD86 as a pro-inflammatory macrophage-associated marker, and CD206 as an anti-inflammatory macrophage-associated marker. (**B**) Quantitative analysis of F4/80-positive cells. (**C**) Quantitative analysis of CD86-positive cells. (**D**) Quantitative analysis of the CD86/F4/80 marker ratio. (**E**) Quantitative analysis of CD206-positive cells. (**F**) Quantitative analysis of the CD206/F4/80 marker ratio. (**G**) CD86/CD206 marker ratio. $n = 3$ mice per group. Data are presented as mean ± SD. ## $p < 0.01$ versus the CON group; ** $p < 0.01$ versus the LPS group.

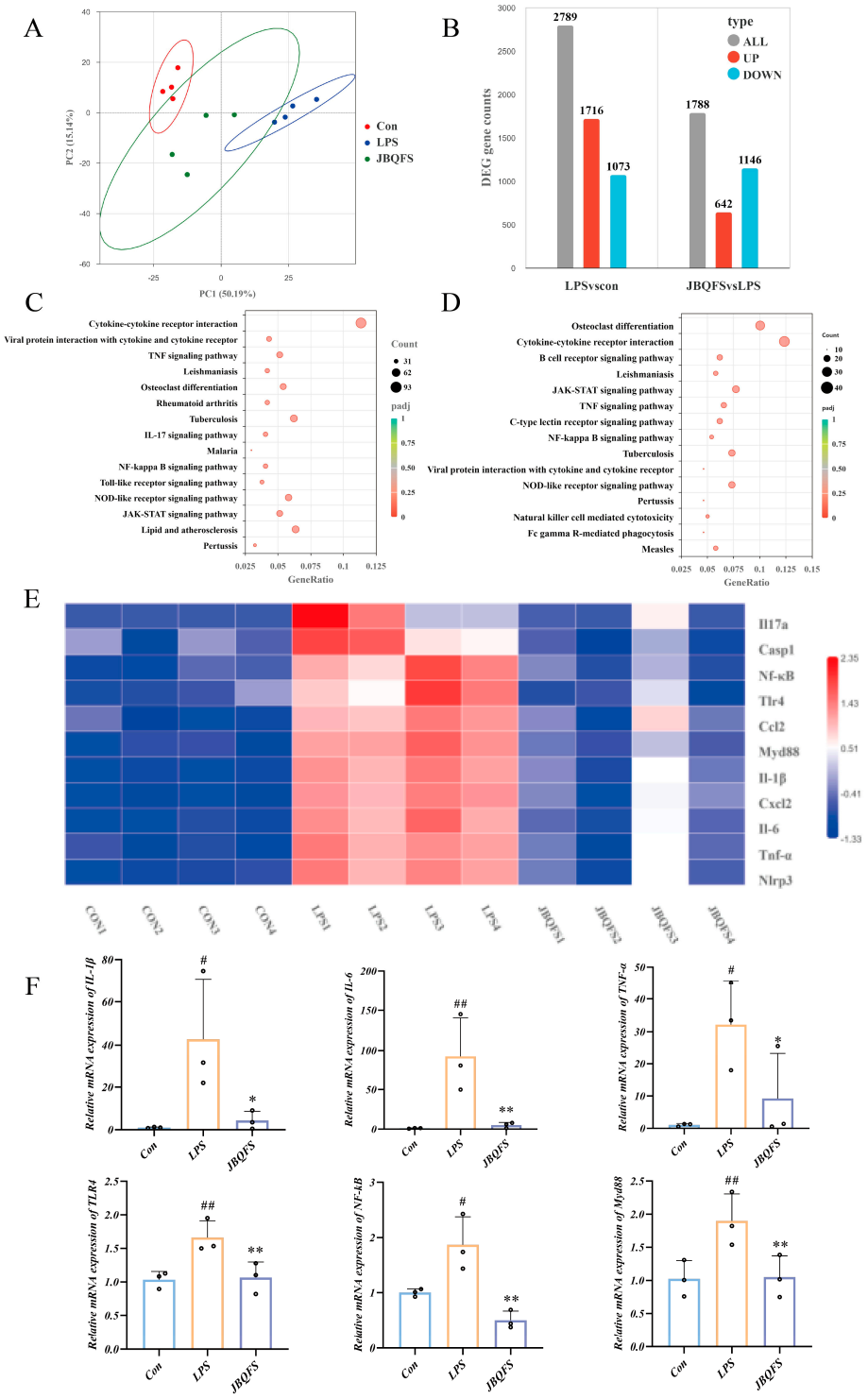


Figure 5. JBQFS regulated inflammation- and immune-related gene expression in lung tissues of LPS-induced ALI mice. (**A**) Principal component analysis. (**B**) Numbers of upregulated and downregulated DEGs in the LPS versus CON and JBQFS-H versus LPS comparisons. (**C**) KEGG enrichment analysis of DEGs in the LPS versus CON comparison. (**D**) KEGG enrichment analysis of DEGs in the JBQFS-H versus LPS comparison. (**E**) Heatmap of representative inflammation- and immune-related genes. (**F**) qRT-PCR validation of selected inflammation-related genes. Transcriptomic analyses in panels A–E were performed using four mice per group ($n = 4$ biological replicates) from the CON, LPS, and JBQFS-H groups. qRT-PCR validation in panel F was performed using three mice per group ($n = 3$ biological replicates) from the same experimental groups. Data in F are presented as mean ± SD. # $p < 0.05$ and ## $p < 0.01$ versus the CON group; * $p < 0.05$ and ** $p < 0.01$ versus the LPS group.

2.7. JBQFS Suppresses LPS-Induced Inflammatory Responses in MH-S Cells

We next established an inflammatory injury model using MH-S cells to investigate the regulatory effects of JBQFS on macrophages during inflammatory responses. First, to evaluate the safety profile of JBQFS, cell viability was assessed by CCK-8 assay after exposure to various concentrations of JBQFS. CCK-8 analysis showed that JBQFS did not significantly affect MH-S cell viability at concentrations up to 1000 μg/mL. In contrast, cell viability decreased to 75.8 ± 6.1% and 68.6 ± 2.0% at 2000 and 4000 μg/mL, respectively. An IC_{50} value could not be determined within the tested concentration range because cell viability remained above 50% at the highest concentration tested (4000 μg/mL). Based on these results, 250, 500, and 1000 μg/mL were selected for subsequent experiments.

The anti-inflammatory activity of JBQFS was further examined in LPS-stimulated MH-S cells by assessing IL-6, TNF-α, IL-1β, and NO production. LPS stimulation increased both the secretion and mRNA expression of IL-6, TNF-α, and IL-1β ($p < 0.05$; Figure 6). JBQFS treatment reduced these cytokine responses compared with the LPS group ($p < 0.05$). In addition, LPS markedly elevated NO production, which was effectively reversed by JBQFS pretreatment ($p < 0.01$). Collectively, these results indicate that JBQFS attenuates inflammatory responses by suppressing the expression of pro-inflammatory mediators in macrophages.

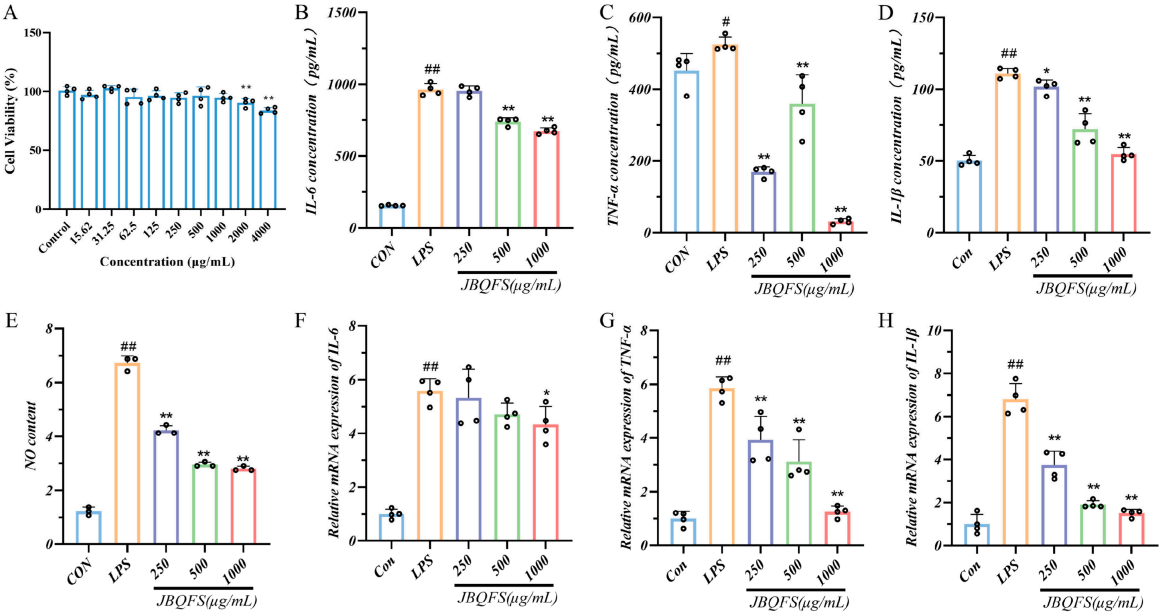


Figure 6. JBQFS inhibited LPS-induced inflammatory responses in MH-S cells. (**A**) Cell viability of MH-S cells after treatment with different concentrations of JBQFS for 24 h, as determined by CCK-8 assay. (**B**–**D**) The concentrations of IL-6, TNF-α, and IL-1β in cell culture supernatants were measured after LPS stimulation with or without JBQFS treatment. (**E**) NO production in the culture supernatant. (**F**–**H**) Relative mRNA expression levels of *Il-6*, *Tnf-α*, and *Il-1β* in MH-S cells. For the inflammatory model, cells were pretreated with JBQFS at 250, 500, or 1000 μg/mL and then stimulated with LPS. $n = 4$ independent biological replicates for all analyses. Data are presented as mean ± SD. # $p < 0.05$ and ## $p < 0.01$ versus the CON group; * $p < 0.05$ and ** $p < 0.01$ versus the LPS group.

2.8. JBQFS Alters Phenotype-Associated Markers and Oxidative Responses in MH-S Cells

Macrophages exhibit heterogeneous activation states in response to inflammatory stimuli. To assess whether JBQFS alters macrophage-associated phenotypic markers, the expression of CD80, CD86, and CD206 in MH-S cells was analyzed by flow cytometry. As shown in Figure 7A–D, LPS increased the proportions of CD80- and CD86-positive cells ($p < 0.01$), whereas JBQFS pretreatment reduced both populations ($p < 0.01$). In contrast, the propor-

tion of CD206-positive cells decreased following LPS stimulation but increased after JBQFS treatment ($p < 0.05$), with the largest change observed in the high-dose group ($p < 0.01$).

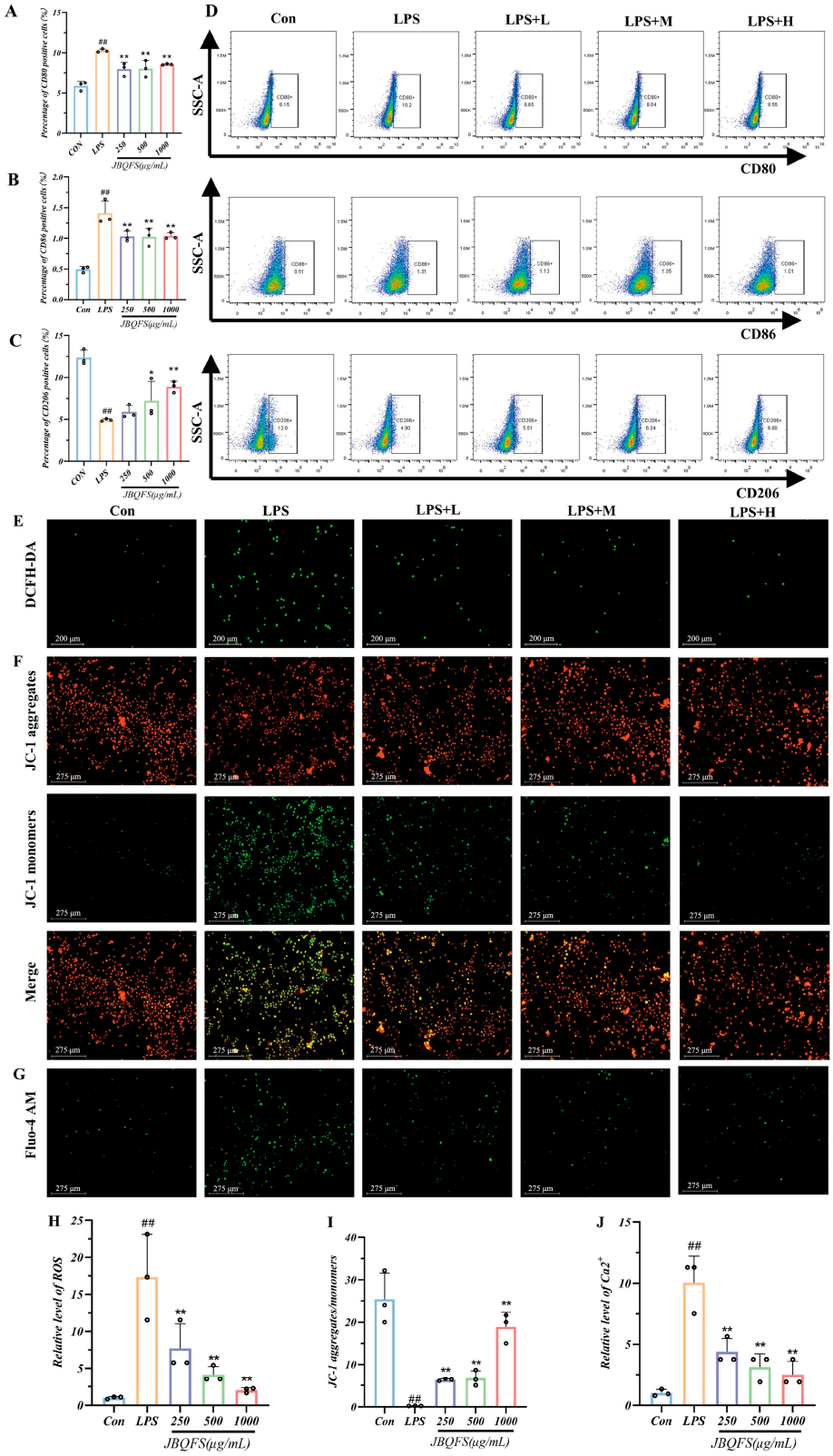


Figure 7. JBQFS modulated macrophage-associated phenotypic markers and cellular stress responses in LPS-stimulated MH-S cells. (**A**–**C**) Percentages of $CD80^+$, $CD86^+$, and $CD206^+$ cells, respectively. (**D**) Representative flow cytometry plots of CD80, CD86, and CD206 expression. (**E**–**G**) Representative

fluorescence images of intracellular ROS (DCFH-DA), mitochondrial membrane potential (JC-1), and intracellular Ca^{2+} (Fluo-4 AM), respectively. (**H**–**J**) Quantification of ROS fluorescence intensity, the JC-1 aggregate/monomer fluorescence ratio, and Ca^{2+} fluorescence intensity, respectively. MH-S cells were pretreated with JBQFS (250, 500, or 1000 μg/mL) before LPS stimulation. Data are presented as mean ± SD ($n = 3$ independent biological replicates per group). ## $p < 0.01$ versus the CON group; * $p < 0.05$ and ** $p < 0.01$ versus the LPS group.

To evaluate the antioxidant capacity of JBQFS, intracellular ROS levels were measured by fluorescent probe staining. As presented in Figure 7E, minimal ROS was detected in untreated cells, whereas LPS stimulation substantially increased green fluorescence intensity, indicating ROS overproduction. JBQFS treatment, particularly at the high dose, markedly attenuated this increase ($p < 0.01$). Mitochondrial membrane potential was subsequently assessed using JC-1 staining. In healthy MH-S cells, JC-1 aggregates emitted strong red fluorescence, while LPS caused a shift to green fluorescence, indicating mitochondrial depolarization ($p < 0.01$). Notably, JBQFS reversed this shift by restoring red fluorescence and reducing green fluorescence ($p < 0.01$). LPS also induced a significant elevation in intracellular Ca^{2+}, which was significantly attenuated by JBQFS ($p < 0.01$). These results show that JBQFS modulated several oxidative and mitochondrial readouts in LPS-stimulated MH-S cells.

3. Discussion

ALI is an acute inflammatory lung syndrome for which effective pharmacological options remain limited [32]. Thus, there is a pressing need for novel and effective therapeutic strategies to improve patient outcomes. TCM formulations have attracted increasing attention for their potential anti-inflammatory and immunomodulatory activities in respiratory disorders [33]. The JBQFS formula comprises seven Chinese herbs with established anti-inflammatory properties and traditional use in respiratory disorders. Previous studies of Xuanfei Baidu Decoction and Shiwei Qingwen Decoction have associated their protective effects against ALI with the regulation of inflammatory signaling pathways. In comparison, our study provides formulation-specific pharmacological evidence for JBQFS by integrating pulmonary injury assessments with macrophage-associated and transcriptional responses, without establishing a direct molecular mechanism.

Inflammatory and oxidative responses contribute to pulmonary tissue damage during ALI [34]. LPS-induced injury is accompanied by vascular dysfunction and inflammatory cell infiltration [17]. Macrophage-derived inflammatory mediators further promote immune cell recruitment [35,36], exacerbating epithelial damage and pulmonary edema [18,37]. In our LPS-induced ALI model, histopathological examination, the lung W/D ratio, inflammatory cytokine measurements, and WBP-derived respiratory parameters demonstrated pulmonary injury following LPS challenge. JBQFS pretreatment attenuated histopathological injury, pulmonary edema, and inflammatory responses. However, respiratory responses varied across parameters and doses, with TV, MV, and TB showing no consistent dose-dependent pattern. These findings support the protective effects of JBQFS against experimental ALI while highlighting variability in respiratory outcomes.

During ALI, recruited macrophages and neutrophils contribute to sustained inflammatory cytokine production [38]. TNF-α can amplify inflammatory responses [39], IL-1β contributes to downstream cytokine signaling [40], and elevated IL-6 is associated with further inflammatory cell recruitment and tissue injury [41]. In our study, JBQFS reduced TNF-α, IL-1β, and IL-6 levels in LPS-challenged mice and MH-S cells. MDA, SOD, and GSH-Px are commonly used to assess oxidative damage and antioxidant defense [42,43], while excessive ROS production can impair mitochondrial function [44] and amplify inflammatory responses [45]. JBQFS decreased MDA levels and increased SOD and GSH-Px

activities in vivo. In MH-S cells, JBQFS reduced intracellular ROS and Ca^{2+} signals and attenuated mitochondrial depolarization. In comparison, a recent study reported that inhalable PD-L1-engineered hybrid cellular vesicles alleviated lung ischemia–reperfusion injury and pneumonia by suppressing neutrophil activation and restoring mitochondrial homeostasis [46]. However, differences in formulation, administration route, and experimental models preclude direct comparisons of therapeutic efficacy. Overall, these findings indicate that JBQFS treatment was associated with reduced inflammatory and oxidative responses, although the cellular observations do not establish a direct mechanism of protection in vivo.

Transcriptomic analysis further provided molecular clues associated with the protective effects of JBQFS. Pathway enrichment analysis linked the differentially expressed genes to several inflammation-related pathways, including cytokine–cytokine receptor interaction, TNF signaling, NF-κB signaling, Toll-like receptor signaling, NOD-like receptor signaling, and JAK–STAT signaling. qRT-PCR further confirmed changes in representative inflammation-related genes, including IL-6, TNF-α, IL-1β, TLR4, MyD88, and NF-κB-related genes. TLR4/MyD88/NF-κB signaling is an important component of inflammatory responses during experimental lung injury [47,48]. In the present study, JBQFS administration was associated with changes in TLR4/MyD88/NF-κB-related gene expression. However, because the present evidence was limited to transcriptomic and mRNA-level analyses, these findings indicate transcriptional associations rather than direct regulation of the signaling pathway.

Macrophage-associated inflammatory responses contribute to the progression and resolution of ALI [49,50]. Pro-inflammatory macrophage responses exacerbate tissue injury through cytokine production and oxidative stress [51,52]. In contrast, macrophages exhibiting anti-inflammatory phenotypes can produce IL-10 and TGF-β, limit inflammatory responses, and promote tissue repair [39]. Their clearance of apoptotic neutrophils may further facilitate inflammation resolution [53]. Wang et al. reported that airway epithelial cell-derived exosomal MEG3 promoted M1 macrophage polarization and pyroptosis through TREM-1-related signaling in a COPD model [54]. In our study, LPS challenge increased CD86-associated signals and decreased CD206-associated signals in lung tissues, whereas JBQFS pretreatment attenuated these changes. Consistently, JBQFS reduced the proportions of CD80- and CD86-positive MH-S cells while increasing the proportion of CD206-positive cells. The immunomodulatory effects of herbal formulations on macrophage responses have also been reported for Shengjiang San, which modulated macrophage polarization through Lactobacillus murinus-derived IAAld and NF-κB/TGF-β signaling in sepsis-induced intestinal injury [55]. However, the observed changes in macrophage-associated markers alone cannot establish definitive polarization states or the molecular mechanisms underlying JBQFS action.

Several limitations should be acknowledged. First, the absence of a pharmacological positive-control group precluded direct comparison of JBQFS with an established anti-inflammatory treatment. Second, the in vivo doses were expressed as crude-herb equivalents, whereas the in vitro concentrations represented the lyophilized JBQFS extract. These exposure measures are not directly comparable, and the cellular experiments should therefore be interpreted as complementary evidence rather than direct confirmation of the in vivo effects. Third, whole-lung immunofluorescence could not distinguish tissue-resident alveolar macrophages from recruited monocyte-derived macrophages, and changes in CD86- and CD206-associated signals alone cannot establish macrophage polarization states. Furthermore, transcriptomic and qRT-PCR analyses identified inflammation-related transcriptional changes but did not establish direct regulation of TLR4/MyD88/NF-κB signaling. Amplification efficiencies and β-actin stability under LPS stimulation were not independently validated, which may affect the interpretation of relative gene expression.

Finally, the limited number of biological replicates for certain endpoints may reduce statistical precision. Further studies incorporating reference treatments, macrophage-specific functional analyses, and protein-level pathway validation are warranted.

Our findings indicate that JBQFS alleviates LPS-induced ALI in association with reduced pulmonary inflammation, oxidative stress, and changes in macrophage-associated inflammatory phenotypes. Transcriptomic and qRT-PCR analyses further identified changes in inflammation-related transcriptional responses, including TLR4/MyD88/NF-κB-related genes. A schematic summary of the experimental findings is shown in Figure 8.

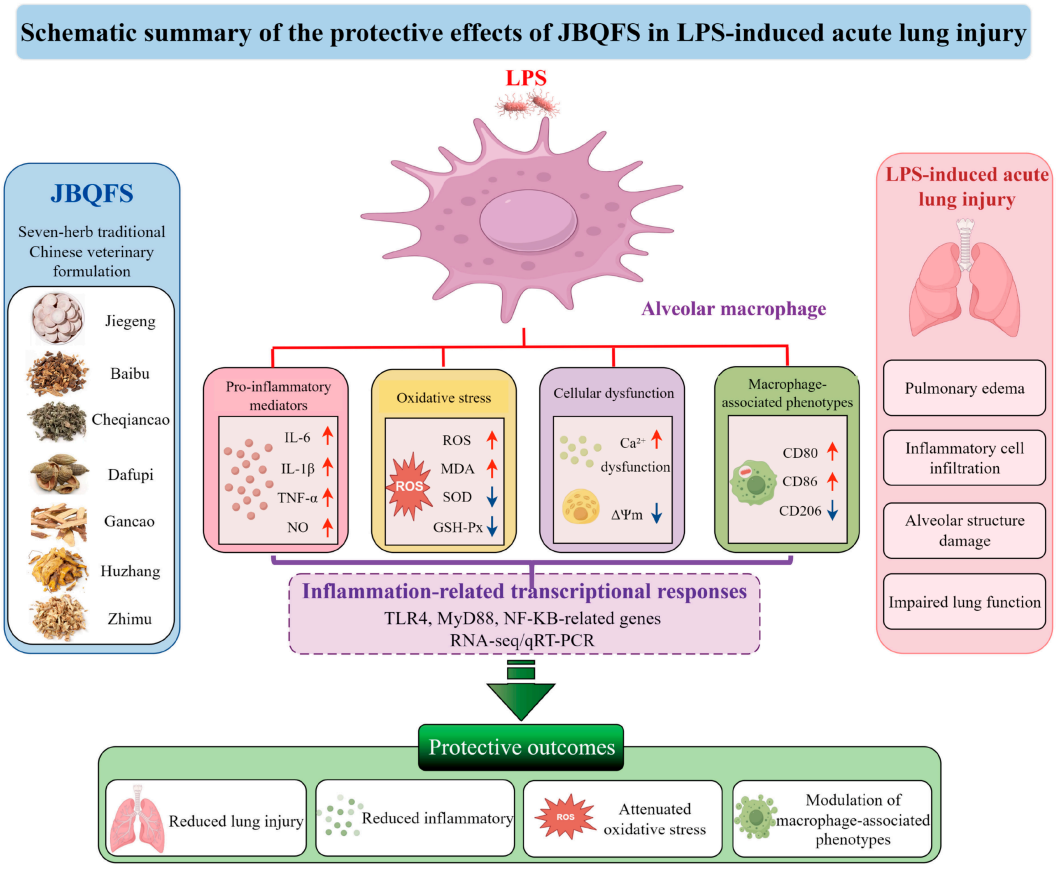


Figure 8. Schematic summary of the proposed protective effects of JBQFS against LPS-induced acute lung injury. LPS-induced acute lung injury was associated with increased pro-inflammatory mediators, oxidative stress, cellular dysfunction, and alterations in macrophage-associated phenotypic markers. JBQFS pretreatment attenuated these responses, as reflected by reduced TNF-α, IL-6, IL-1β, NO, ROS, and MDA levels, increased SOD and GSH-Px activities, reduced intracellular Ca^{2+} accumulation, preservation of mitochondrial membrane potential, and modulation of CD80-, CD86-, and CD206-associated markers. Transcriptomic and qRT-PCR analyses further identified changes in inflammation-related transcriptional responses, including TLR4/MyD88/NF-κB-related genes. The involvement of this signaling pathway was not functionally validated and is therefore presented as an associated transcriptional response rather than an established mechanism of JBQFS action.

4. Materials and Methods

4.1. Chemicals and Reagents

All crude herbal materials used in this study were purchased from Bozhou Zhenshang Pharmaceutical Co., Ltd. (Bozhou, Anhui, China). The geographic origins and batch numbers of the individual herbal materials are provided in Table 2. The individual herbal materials were supplied with manufacturer quality-control documentation and complied with the corresponding requirements of the Chinese Pharmacopoeia.

Table 2. Composition and traceability information of JBQFS.

Pinyin Name	Botanical Source	Medicinal Part	Proportion (g)	Origin	Batch No.
Jiegeng	*Platycodon grandiflorus* (Jacq.) A.DC	Root	60	Bozhou, Anhui, China	240601
Baibu	*Stemona japonica* (Blume) Miq	Root	30	Yichang, Hubei, China	240901
Cheqiancao	*Plantago asiatica* L.	Whole herb	60	Xixia, Henan, China	240201
Dafupi	*Areca catechu* L.	Pericarp	45	Ruili, Yunnan, China	240302
Gancao	*Glycyrrhiza uralensis* Fisch. ex DC	Root and rhizome	45	Dingxi, Gansu, China	240802
Huzhang	*Reynoutria japonica* Houtt	Rhizome and root	50	Yichun, Jiangxi, China	240601
Zhimu	*Anemarrhena asphodeloides* Bunge	Rhizome	90	Anguo, Hebei, China	240802

Note: The scientific names and taxonomic authorities of the medicinal plants were verified using authoritative botanical databases.

Lipopolysaccharide (LPS; Escherichia coli O111:B4; Cat. No. S1732-25mg), JC-1 (Cat. No. C2005), DCFH-DA (Cat. No. S1105M), Fluo-4 AM (Cat. No. S1060), and a nitric oxide assay kit (Cat. No. S0021S) were purchased from Beyotime Biotechnology Co., Ltd. (Shanghai, China). Mouse IL-6 (Cat. No. EK206), TNF-α (Cat. No. EK282), and IL-1β (Cat. No. EK201B) ELISA kits were purchased from Hangzhou Lianke Biotechnology Co., Ltd. (Hangzhou, China). The SOD activity assay kit (Cat. No. BC5165) and MDA assay kit (Cat. No. BC0025) were obtained from Solarbio Science & Technology Co., Ltd. (Beijing, China), and the GSH-Px assay kit (Cat. No. ADS-W-G003) was obtained from Jiangsu Aidisheng Biotechnology Co., Ltd. (Yancheng, Jiangsu, China). Protein concentrations were determined using a BCA Protein Quantification Kit (Cat. No. KTD3001; Abbkine Biotechnology Co., Ltd., Wuhan, China).

For lung-tissue multiplex immunofluorescence staining, antibodies against CD86 (Cat. No. 19589) and CD206 (Cat. No. 24595) were purchased from Cell Signaling Technology (Danvers, MA, USA), and the F4/80 antibody (Cat. No. ab300421) was obtained from Abcam (Cambridge, UK). The MaxVision™ HRP-Polymer anti-Rabbit IHC Kit (Cat. No. KIT-5005) was obtained from Fuzhou Maixin Biotech Co., Ltd. (Fuzhou, China). Fluorescein tyramide (Cat. No. 11062), Cy3 tyramide (Cat. No. 11065), and Cy5 tyramide (Cat. No. 11066) were purchased from AAT Bioquest (Sunnyvale, CA, USA), and DAPI staining solution (Cat. No. KGA215) was obtained from KeyGEN BioTECH (Nanjing, China).

For flow-cytometric analysis, FITC-conjugated anti-mouse CD80 (Cat. No. E-AB-F0992C), APC-conjugated anti-mouse CD86 (Cat. No. E-AB-F0994E), and PE-conjugated anti-mouse CD206/MMR (Cat. No. E-AB-F1135D) antibodies were obtained from Elabscience Biotechnology Co., Ltd. (Wuhan, China). The Cell Counting Kit-8 (Cat. No. C6005) was obtained from NCM Biotech (Suzhou Xinsaimai Biotechnology Co., Ltd., Suzhou, China). RPMI-1640 medium (Cat. No. C11875500BT) was purchased from Gibco (Thermo Fisher Scientific (China) Co., Ltd., Shanghai, China), and fetal bovine serum (Cat. No. FSD500) was obtained from ExCell Bio (Suzhou ExCell Biotechnology Co., Ltd., Taicang, Jiangsu, China).

4.2. Preparation of JBQFS

The JBQFS formulation was prepared according to the composition and proportions of the medicinal materials shown in Table 2. A total of 380 g of the mixed crude herbs was soaked in 10 volumes (v/w) of deionized water for 30 min and decocted under mild heat for 1.5 h. The first decoction was collected by filtration. The residue was re-extracted with 5 volumes (v/w) of deionized water for 1 h and filtered to obtain the second decoction. The two filtrates were combined and concentrated to a final volume of 380 mL, corresponding to 1 g crude-herb equivalent/mL. The concentrated decoction was lyophilized, yielding

137 g of powdered extract, corresponding to an extraction yield of 36.1% (*w*/*w*) relative to the initial crude-herb weight. The lyophilized extract was stored at −20 °C until use.

4.3. UHPLC-HRMS/MS Analysis of JBQFS

JBQFS powder (300 mg) was dissolved in 1 mL of methanol, sonicated in an ice bath for 20 min, and centrifuged at 12,000× *g* for 20 min at 4 °C. The supernatant was analyzed using an X500R high-resolution mass spectrometer coupled to a UHPLC system (AB Sciex LLC, Marlborough, MA, USA), with data acquisition controlled by SCIEX OS software (version 5.0).

Chromatographic separation was performed at 50 °C with a flow rate of 0.30 mL/min and an injection volume of 4 µL. Positive-ion analysis employed a Waters ACQUITY UPLC BEH C8 column (1.7 µm, 2.1 × 100 mm) with 0.1% formic acid in water (A) and acetonitrile (B), whereas negative-ion analysis employed a Waters ACQUITY UPLC HSS T3 column (1.8 µm, 2.1 × 100 mm) with 6.5 mM ammonium bicarbonate in water (A) and 90% methanol (B). The gradient increased from 5% to 99% B over 2–37 min, followed by 100% B (positive mode) or 99% B (negative mode) at 37–42 min and re-equilibration at 5% B until 45 min.

MS^1 and MS/MS data were acquired over *m*/*z* 70–1050 and 50–1050, respectively, with information-dependent acquisition (IDA) in positive-ion mode and data-dependent acquisition (DDA) in negative-ion mode. Data were processed using MS-DIAL for spectral-library/database searching. Compound annotations were considered tentative, with identification confidence reported in Table 1. Glycyrrhizic acid and polydatin were independently quantified by HPLC in three JBQFS batches, as detailed in Supplementary Method S1, Table S1, and Figures S1 and S2.

4.4. Animal Experiment

Male SPF BALB/c mice, 6 weeks of age and weighing 17 ± 1 g, were obtained from the Comparative Medicine Center of Yangzhou University (Yangzhou, Jiangsu, China). Animals were housed under SPF conditions at the Laboratory Animal Center of Nanjing Agricultural University (Nanjing, Jiangsu, China), with a 12 h light/dark cycle and free access to food and water. A 1-week acclimation period was allowed before the experiment. All experimental procedures were reviewed and approved by the Institutional Animal Care and Use Committee of Nanjing Agricultural University (protocol code NJAULLSC2025004; approval date: 3 January 2025) and were performed in accordance with institutional animal care guidelines.

After acclimation, mice were assigned to five groups ($n = 10$ per group) according to a computer-generated randomization sequence: the control group (CON), LPS model group (LPS), and low- (JBQFS-L), medium- (JBQFS-M), and high-dose (JBQFS-H) JBQFS groups, receiving 2, 4, and 8 g/kg, respectively. The initial allocation of 10 mice per group was selected to accommodate the planned terminal sampling procedures and to provide the required biological replicates for the different experimental endpoints. All JBQFS doses were expressed as crude-herb equivalents. Dose selection was based on the veterinary clinical dose of JBQFS used in calves (0.5 g/kg). For a representative 100-kg calf, body surface area was estimated as $0.14 \times 100^{0.57} = 1.93$ m^2, corresponding to a Km value of approximately 51.8 kg/m^2. With a mouse Km value of 3, the mouse-equivalent dose was calculated as $0.5 \times 51.8/3 \approx 8.6$ g/kg [56,57]. Accordingly, 8 g/kg was selected as the high dose, with 4 and 2 g/kg used as the medium and low doses, respectively.

Mice in the JBQFS groups received the assigned dose once daily by oral gavage for 5 consecutive days, whereas CON and LPS mice received an equivalent volume of distilled water. One hour after the final gavage, mice were anesthetized by intraperitoneal injection of 2.5% Avertin (0.25 mL per mouse). ALI was then induced by intranasal instillation

of LPS derived from *Escherichia coli* O111:B4 (4 mg/kg; Cat. No. S1732-25mg; Beyotime Biotechnology Co., Ltd., Shanghai, China) in a total volume of 20 μL. Mice in the CON group received an equivalent volume of normal saline.

At 12 h after LPS challenge, mice were euthanized and allocated to different terminal sampling procedures according to the requirements of each endpoint. Four mice per group were used for BALF collection and lung wet-to-dry weight determination, with one lung used for lavage and the contralateral non-lavaged lung used for wet-to-dry weight analysis. Lung tissues from the remaining animals were allocated to biochemical, molecular, histopathological, and immunofluorescence analyses. Four biological replicates per group were used for transcriptomic analysis in the CON, LPS, and JBQFS-H groups, whereas three biological replicates per group were used for histopathological and immunofluorescence analyses. Where technically compatible, different lung lobes from the same animal were allocated to different tissue-based analyses. The exact number of biological replicates analyzed for each endpoint is specified in the corresponding figure legend. No animals were excluded after randomization or from the final analyses.

4.5. Evaluation of Lung Wet-to-Dry Weight Ratio

The non-lavaged lung tissues from four mice per group were used for determination of the lung wet-to-dry weight ratio. Fresh lung samples were gently rinsed with PBS, blotted to remove surface moisture, and weighed immediately as the wet weight. The tissues were subsequently dried at 60 °C for 48 h until dry-weight measurement. The W/D ratio was obtained by dividing the wet weight by the corresponding dry weight.

4.6. Assessment of Respiratory Parameters

Respiratory parameters were assessed by whole-body plethysmography (WBP) using an EMMSLink system (Laboratory Instrumentation Limited, trading as EMMS, Alton, Hampshire, UK) at 12 h after LPS challenge. Following system calibration, conscious mice were individually placed in the plethysmography chambers and allowed to acclimatize for 3–5 min. Tidal volume (TV), minute ventilation (MV), peak expiratory flow (PEF), enhanced pause (Penh), and total breath duration (TB) were continuously recorded. TV represents the estimated volume of air exchanged per breath, MV the estimated ventilation per minute, PEF the maximum expiratory flow, and TB the duration of a complete respiratory cycle. Penh was treated as a dimensionless respiratory waveform-derived index rather than a direct measure of airway resistance. No single WBP-derived parameter was prespecified as the primary functional outcome; the measurements were interpreted collectively as complementary respiratory readouts. Data were collected at 10-s intervals over a 20-min recording period and subsequently exported for statistical analysis.

4.7. Collection and Processing of Bronchoalveolar Lavage Fluid (BALF)

BALF was obtained from four mice per group at 12 h after LPS challenge. Following euthanasia, the trachea was exposed and cannulated with a blunt-ended needle. One lung was lavaged three times with 0.8 mL of ice-cold sterile PBS, whereas the contralateral lung was retained without lavage for wet-to-dry weight determination. Lavage fractions recovered from each mouse were combined and kept on ice before centrifugation at 400× *g* for 10 min at 4 °C. The resulting cell-free supernatants were aliquoted and stored at −80 °C for subsequent measurement of IL-6, TNF-α, and IL-1β concentrations by ELISA.

4.8. H&E and Histopathological Scoring

Lung specimens were immersed in 4% paraformaldehyde for 24 h, followed by routine dehydration in graded ethanol, xylene clearing, and paraffin embedding. Paraffin sections

of 5 μm thickness were prepared, deparaffinized, rehydrated, and subjected to hematoxylin and eosin (H&E) staining.

One H&E-stained lung section from each mouse was evaluated using a semiquantitative histopathological scoring system ranging from 0 to 4 according to the overall severity of lung injury, including alveolar septal thickening, inflammatory cell infiltration, pulmonary edema or hemorrhage, and disruption of alveolar architecture. A score of 0 indicated no apparent pathological changes, whereas scores of 1–4 represented progressively increasing severity of lung injury. Whole-section images were coded before evaluation, and scoring was performed by an independent assessor blinded to the experimental group assignments. Each mouse was considered one independent biological replicate.

4.9. Measurement of Inflammatory Cytokines and Oxidative Stress Parameters

For cytokine analysis, BALF supernatants and serum samples were used to determine the protein levels of IL-6, TNF-α, and IL-1β using commercial ELISA kits according to the manufacturers' instructions. For oxidative stress analysis, lung tissues were homogenized in ice-cold PBS, and the supernatants were collected after centrifugation. Protein concentrations in lung tissue homogenates were determined using a BCA kit for normalization. The activities of SOD and GSH-Px and the levels of MDA in lung tissue homogenates and serum were measured using corresponding assay kits.

4.10. Immunofluorescence Staining

Paraffin-embedded lung sections were deparaffinized and rehydrated before heat-induced antigen retrieval in citrate buffer (pH 6.0). Multiplex immunofluorescence staining was carried out sequentially with a tyramide signal amplification (TSA) system. Sections were incubated with primary antibodies against CD86 (1:400), CD206 (1:800), and F4/80 (1:1000), followed by HRP-polymer detection and TSA-based signal development. CD86, CD206, and F4/80 were visualized with Cy3, Cy5, and fluorescein tyramide, respectively. Nuclei were counterstained with DAPI, and fluorescence images were acquired with an EVOS FL Auto inverted fluorescence microscope (Thermo Fisher Scientific, Waltham, MA, USA). F4/80 served as a macrophage marker, whereas CD86 and CD206 were evaluated as pro-inflammatory and anti-inflammatory macrophage-associated markers, respectively.

4.11. Cell Culture and Viability Assay

The murine alveolar macrophage cell line MH-S was obtained from Wuhan Sewell Biotechnology Co., Ltd. (STCC20007P, Wuhan, China). Cells were cultured in RPMI-1640 supplemented with 10% FBS and 1% P/S at 37 °C in a humidified atmosphere containing 5% CO_2. The lyophilized JBQFS extract was dissolved directly in complete RPMI-1640 medium to obtain the indicated concentrations. Control cells received drug-free complete medium without an additional solvent vehicle.

For the cytotoxicity assay, cells were plated in 96-well plates at 1×10^4 cells per well and allowed to attach for 24 h before exposure to JBQFS at 0–4000 μg/mL for a further 24 h. CCK-8 reagent was added at 10 μL per well, followed by incubation for 2 h, and absorbance was measured at 450 nm using a SPARK multimode microplate reader (Tecan Group Ltd., Männedorf, Switzerland). Based on the cell-viability results, 250, 500, and 1000 μg/mL were selected as the low, medium, and high concentrations, respectively, for subsequent experiments. These concentrations represent the actual concentrations of the lyophilized JBQFS extract in the culture medium.

4.12. Inflammatory Cytokines Determination

Culture supernatants from each group were collected and clarified by centrifugation at 4000× *g* for 5 min at 4 °C. The concentrations of TNF-α, IL-6, and IL-1β in the supernatants were quantified by ELISA, whereas NO levels were determined with the corresponding assay kit following the manufacturer's protocol.

4.13. Flow Cytometric Analysis

To evaluate macrophage-associated phenotypic markers, MH-S cells were plated at 5×10^5 cells/well in 12-well plates and cultured for 24 h. Cells were then assigned to CON, LPS (1 μg/mL), or JBQFS-pretreated (1 h) plus LPS groups. After 24 h, cells were harvested, stained with fluorescence-conjugated antibodies against CD80, CD86, and CD206 (all diluted 1:200) for 30 min at 4 °C in the dark, and analyzed by flow cytometry(BD Biosciences, San Jose, CA, USA).

4.14. Intracellular Reactive Oxygen Species (ROS) Measurement

Intracellular ROS production was evaluated with the DCFH-DA fluorescent probe. After 24 h of JBQFS treatment, cells were loaded with 10 μmol/L DCFH-DA in serum-free medium and incubated at 37 °C for 20 min in the dark. Excess probe was removed by three washes with serum-free medium, after which fluorescence images were acquired with an inverted fluorescence microscope (Thermo Fisher Scientific, Waltham, MA, USA).

4.15. Intracellular Ca^{2+} Level Determination

Intracellular Ca^{2+} was evaluated with the Fluo-4 AM fluorescent probe. After 24 h of treatment, cells were incubated with 300 μL of Fluo-4 AM working solution at 37 °C for 30 min in the dark. The cells were subsequently washed with PBS, and fluorescence images were acquired with an inverted fluorescence microscope (Thermo Fisher Scientific, Waltham, MA, USA).

4.16. Mitochondrial Membrane Potential Determination

Mitochondrial membrane potential was evaluated using the JC-1 fluorescent probe. After 24 h of treatment, cells were incubated with JC-1 working solution at 37 °C for 20 min in the dark. Excess probe was removed by washing with PBS, and fluorescence images were subsequently acquired with an inverted fluorescence microscope (Thermo Fisher Scientific, Waltham, MA, USA). Mitochondrial membrane potential was evaluated according to the ratio of JC-1 aggregate fluorescence to monomer fluorescence.

4.17. Quantitative Reverse Transcription PCR (qRT-PCR) Analysis

Total RNA from MH-S cells and lung tissues was extracted with TsingZol Total RNA Extraction Reagent (Cat. No. TSP401; Tsingke Biotechnology Co., Ltd., Beijing, China). The resulting RNA was reverse-transcribed into cDNA with the Evo M-MLV Mix Kit with gDNA Clean for qPCR (Cat. No. AG11728; Accurate Biotechnology (Hunan) Co., Ltd., Changsha, China). qRT-PCR was performed on a StepOnePlus Real-Time PCR System (Applied Biosystems, Foster City, CA, USA) with the SYBR Green Premix Pro Taq HS qPCR Kit (Cat. No. AG11701; Accurate Biotechnology (Hunan) Co., Ltd., Changsha, China). The amplification program consisted of an initial denaturation at 95 °C for 30 s, followed by 40 cycles of 95 °C for 5 s and 60 °C for 30 s. A dissociation curve analysis was performed at the end of amplification. Gene expression was normalized to β-actin and calculated using the $2^{-\Delta\Delta Ct}$ method. Amplification efficiencies were not experimentally determined by standard-curve analysis, and the stability of β-actin under LPS stimulation was not independently validated. Primer sequences and amplicon sizes are provided in Table 3.

Table 3. Primer sequences used for qRT-PCR.

Primer Name	Primer Sequence (5′–3′)		Amplicon Size (bp)
	Forward Primer	Reverse Primer	
β-actin	CGTTGACATCCGTAAAGACC	AACAGTCCGCCTAGAAGCAC	281
IL-1β	TGCCACCTTTTGACAGTGATG	TTCTTGTGACCCTGAGCGAC	94
IL-6	CCAAGAGGTGAGTGCTTCCC	CTGTTGTTCAGACTCTCTCCCT	118
TNF-α	CAGGCGGTGCCTATGTCTC	CGATCACCCCGAAGTTCAGTAG	89
TLR4	GGACTATGTGATGTGACCATTGAT	TTATAGATACACCTGCCAGAGACA	124
NF-κB	GGATGACAGAGGCGTGTATTAG	CCTTCTCTCTGTCTGTGAGTTG	114
MyD88	TCATGTTCTCCATACCCTTGGT	AAACTGCGAGTGGGGTCAG	175

4.18. RNA Sequencing and Bioinformatic Analysis

To further explore the potential molecular basis underlying the protective effects of JBQFS, RNA sequencing was performed using lung tissues from the CON, LPS, and JBQFS-H groups, with four biological replicates per group. Total RNA was extracted from lung tissues, and RNA integrity was assessed using an Agilent Bioanalyzer 2100 system (Agilent Technologies, Santa Clara, CA, USA). Qualified RNA samples were used for library construction and sequenced on an Illumina NovaSeq platform (Illumina, Inc., San Diego, CA, USA) to generate 150 bp paired-end reads.

Raw sequencing data were filtered with fastp to exclude adaptor contamination, poly-N-containing reads, and low-quality sequences. The resulting clean reads were mapped to the mouse reference genome with HISAT2 v2.0.5, followed by transcript assembly with StringTie v1.3.3b. Gene-level read counts were generated with featureCounts v1.5.0-p3 and subsequently analyzed for differential expression using the DESeq2 R package. For visualization of gene expression, expression abundance was additionally expressed as fragments per kilobase of transcript per million mapped reads (FPKM). Genes with adjusted p values < 0.05 and $|\log_2 \text{fold change}| > 1$ were defined as differentially expressed genes (DEGs). Gene Ontology (GO) and Kyoto Encyclopedia of Genes and Genomes (KEGG) enrichment analyses were performed using the clusterProfiler R package. The raw RNA-sequencing data generated in this study have been deposited in the NCBI Sequence Read Archive (SRA) under BioProject accession PRJNA1554958.

4.19. Statistical Analysis

Data for continuous variables are presented as mean ± SD. For animal experiments, each mouse was considered an independent biological replicate, and the exact number of animals analyzed for each endpoint is specified in the corresponding figure legend. Four biological replicates per group were used for transcriptomic analysis. For the MH-S cell experiments, four independent biological replicates were used for the cell-viability, inflammatory mediator, and qRT-PCR analyses shown in Figure 6, whereas three independent biological replicates were used for the flow-cytometric and fluorescence-based cellular stress analyses shown in Figure 7.

Group differences in continuous endpoints were analyzed by one-way ANOVA with Tukey's multiple-comparison test. When a nonparametric approach was required, the Kruskal–Wallis test followed by Dunn's multiple-comparison test was applied. Histopathological lung injury scores were analyzed as ordinal data and are presented as individual animal values with the median; group differences were evaluated using the Kruskal–Wallis test followed by Dunn's multiple-comparison test. Post hoc p values were adjusted within each endpoint by the corresponding Tukey or Dunn procedure, whereas no additional multiplicity correction was applied across distinct biological endpoints. For transcriptomic analysis, DESeq2-adjusted p values were used to identify differentially expressed genes. Statistical analyses were conducted in GraphPad Prism 8.0.2 (GraphPad Software, San Diego,

CA, USA), with $p < 0.05$ considered statistically significant. For each biological replicate, ELISA measurements were performed in technical duplicate and qRT-PCR measurements in technical triplicate; technical replicates were averaged before statistical analysis.

5. Conclusions

Collectively, the present study demonstrates that JBQFS protects against experimental LPS-induced ALI. JBQFS pretreatment alleviated pulmonary histopathological injury, ameliorated LPS-induced alterations in respiratory parameters, reduced local and systemic inflammatory responses, and attenuated oxidative stress. JBQFS also modulated macrophage-associated phenotypic markers in lung tissue and LPS-stimulated MH-S cells. Transcriptomic and qRT-PCR analyses further identified inflammation-related transcriptional responses, including changes in TLR4/MyD88/NF-κB-related genes, associated with JBQFS administration. These findings provide pharmacological evidence supporting further investigation of JBQFS as a veterinary herbal formulation for inflammatory respiratory disorders.

6. Patents

The JBQFS formulation described in this study is covered by a Chinese invention patent entitled "A traditional Chinese medicine composition, its preparation method, and its application in products for the prevention and treatment of bovine respiratory diseases" (Patent No. ZL202311347908.5; Grant Publication No. CN117138004B). D.W., X.D., and Y.Yu. are listed as inventors of this patent, and Nanjing Agricultural University is the patent holder.

Supplementary Materials: The following supporting information can be downloaded at: https://www.mdpi.com/article/10.3390/ph19111835/s1, Supplementary Method S1: Quantification of marker compounds in JBQFS; Figure S1: HPLC chromatograms for the quantitative determination of glycyrrhizic acid in JBQFS; Figure S2: HPLC chromatograms for the quantitative determination of polydatin in JBQFS; Table S1: Contents of glycyrrhizic acid and polydatin in three batches of JBQFS; Data S1: Complete differential gene expression and KEGG enrichment results for both comparisons.

Author Contributions: X.D.: Writing—original draft, methodology, validation, data curation, formal analysis, visualization. J.H.: Methodology, investigation, validation, data curation. L.Y.: Investigation, methodology, validation. Y.Y. (Yaming Yu): Methodology, investigation. K.F.: Formal analysis, data curation, visualization. Y.Y. (Yang Yang): Writing—review and editing, supervision. D.W.: Conceptualization, supervision, project administration, funding acquisition. All authors have read and agreed to the published version of the manuscript.

Funding: This research was funded by the National Natural Science Foundation of China, grant number 32373053; the Fundamental Research Funds for the Central Universities, grant number QTPY2026009; and the National Key Research and Development Program, grant number 2026FRF05010. The APC was funded by the authors' research group.

Institutional Review Board Statement: The animal study protocol was approved by the Institutional Animal Care and Use Committee of Nanjing Agricultural University (protocol code NJAULLSC2025004; approved on 3 January 2025).

Informed Consent Statement: Not applicable.

Data Availability Statement: The raw RNA-sequencing data generated in this study are openly available in the NCBI Sequence Read Archive (SRA) under BioProject accession number PRJNA1554958 (https://www.ncbi.nlm.nih.gov/bioproject/PRJNA1554958, accessed on 2 November 2026).

Conflicts of Interest: D.W., X.D., and Y.Yu. are inventors of Chinese invention patent ZL202311347908.5 (Grant Publication No. CN117138004B), which covers the JBQFS formulation evaluated in this study. Nanjing Agricultural University is the patent holder. The remaining authors declare no conflicts of

interest. The funders had no role in the design of the study; in the collection, analyses, or interpretation of data; in the writing of the manuscript; or in the decision to publish the results.

Abbreviations

ALI	Acute lung injury
BALF	Bronchoalveolar lavage fluid
BCA	Bicinchoninic acid
DEGs	Differentially expressed genes
GO	Gene Ontology
GSH-Px	Glutathione peroxidase
IL-1β	Interleukin-1β
IL-6	Interleukin-6
JBQFS	Jiebai-Qingfei San
KEGG	Kyoto Encyclopedia of Genes and Genomes
LPS	Lipopolysaccharide
MDA	Malondialdehyde
MyD88	Myeloid differentiation primary response 88
NF-κB	Nuclear factor kappa B
RNA-seq	RNA sequencing
ROS	Reactive oxygen species
qRT-PCR	Quantitative reverse transcription PCR
SOD	Superoxide dismutase
TCM	Traditional Chinese Medicine
TLR4	Toll-like receptor 4
TNF-α	Tumor necrosis factor-α

References

1. Zhu, W.; Zhang, Q.; Jin, L.; Lou, S.; Ye, J.; Cui, Y.; Xiong, Y.; Lin, M.; Liang, G.; Luo, W.; et al. OTUD1 Deficiency Alleviates LPS-Induced Acute Lung Injury in Mice by Reducing Inflammatory Response. *Inflammation* **2025**, *48*, 649–661. [CrossRef] [PubMed]
2. Zhang, J.; Guo, Y.; Mak, M.; Tao, Z. Translational Medicine for Acute Lung Injury. *J. Transl. Med.* **2024**, *22*, 25. [CrossRef] [PubMed]
3. Wang, F.; Ge, R.; Cai, Y.; Zhao, M.; Fang, Z.; Li, J.; Xie, C.; Wang, M.; Li, W.; Wang, X. Oxidative Stress in ARDS: Mechanisms and Therapeutic Potential. *Front. Pharmacol.* **2025**, *16*, 1603287. [CrossRef] [PubMed]
4. Zhang, F.; Li, Y.; Xi, Y.; Zhang, Y.; Wang, L.; Xu, H.; Tian, J.; Guo, F.; Yang, H. Qinbaohong Zhike Oral Liquid Attenuates LPS-Induced Acute Lung Injury in Immature Rats by Inhibiting OLFM4. *Oxidative Med. Cell. Longev.* **2022**, *2022*, 7272371. [CrossRef] [PubMed]
5. Gan, A.; Chen, H.; Lin, F.; Wang, R.; Wu, B.; Yan, T.; Jia, Y. Sanzi Yangqin Decoction Improved Acute Lung Injury by Regulating the TLR2-Mediated NF-κB/NLRP3 Signaling Pathway and Inhibiting the Activation of NLRP3 Inflammasome. *Phytomedicine* **2025**, *139*, 156438. [CrossRef] [PubMed]
6. Mariajoseph-Antony, L.F.; Kannan, A.; Panneerselvam, A.; Loganathan, C.; Shankar, E.M.; Anbarasu, K.; Prahalathan, C. Role of Aquaporins in Inflammation-a Scientific Curation. *Inflammation* **2020**, *43*, 1599–1610. [CrossRef] [PubMed]
7. Li, Y.-L.; Qin, S.-Y.; Li, Q.; Song, S.-J.; Xiao, W.; Yao, G.-D. Jinzhen Oral Liquid Alleviates Lipopolysaccharide-Induced Acute Lung Injury through Modulating TLR4/MyD88/NF-κB Pathway. *Phytomedicine* **2023**, *114*, 154744. [CrossRef] [PubMed]
8. Wang, J.; Luo, J.; Rotili, D.; Mai, A.; Steegborn, C.; Xu, S.; Jin, Z.G. SIRT6 Protects Against Lipopolysaccharide-Induced Inflammation in Human Pulmonary Lung Microvascular Endothelial Cells. *Inflammation* **2024**, *47*, 323–332. [CrossRef] [PubMed]
9. Fernando, S.M.; Ferreyro, B.L.; Urner, M.; Munshi, L.; Fan, E. Diagnosis and Management of Acute Respiratory Distress Syndrome. *Can. Med. Assoc. J.* **2021**, *193*, E761–E768. [CrossRef] [PubMed]
10. Cui, J.; Deng, Y.; Li, X.; Gao, L.; Li, J.; Li, Z.; Qu, H.; Chu, Y.; Gu, Y.; Meng, M.; et al. Herbal-Based Xuebijing Injection Ameliorated Vascular Endothelial Dysfunction via Inhibiting ACLY/MYB/RIG-I Axis in Sepsis-Associated Lung Injury. *Phytomedicine* **2025**, *140*, 156573. [CrossRef] [PubMed]
11. He, Y.-Q.; Zhou, C.-C.; Yu, L.-Y.; Wang, L.; Deng, J.-L.; Tao, Y.-L.; Zhang, F.; Chen, W.-S. Natural Product Derived Phytochemicals in Managing Acute Lung Injury by Multiple Mechanisms. *Pharmacol. Res.* **2021**, *163*, 105224. [CrossRef] [PubMed]
12. Ding, Z.; Zhong, R.; Xia, T.; Yang, Y.; Xing, N.; Wang, W.; Wang, Y.; Yang, B.; Sun, X.; Shu, Z. Advances in Research into the Mechanisms of Chinese Materia Medica against Acute Lung Injury. *Biomed. Pharmacother.* **2020**, *122*, 109706. [CrossRef] [PubMed]

13. Ma, Y.; Xu, H.; Chen, G.; Liu, W.; Ma, C.; Meng, J.; Yuan, L.; Hua, X.; Ge, G.; Lei, M. Uncovering the Active Constituents and Mechanisms of Rujin Jiedu Powder for Ameliorating LPS-Induced Acute Lung Injury Using Network Pharmacology and Experimental Investigations. *Front. Pharmacol.* **2023**, *14*, 1186699. [CrossRef] [PubMed]
14. Wang, Y.; Wang, X.; Li, Y.; Xue, Z.; Shao, R.; Li, L.; Zhu, Y.; Zhang, H.; Yang, J. Xuanfei Baidu Decoction Reduces Acute Lung Injury by Regulating Infiltration of Neutrophils and Macrophages via PD-1/IL17A Pathway. *Pharmacol. Res.* **2022**, *176*, 106083. [CrossRef] [PubMed]
15. Zhu, Y.; Luo, L.; Zhang, M.; Song, X.; Wang, P.; Zhang, H.; Zhang, J.; Liu, D. Xuanfei Baidu Formula Attenuates LPS-Induced Acute Lung Injury by Inhibiting the NF-κB Signaling Pathway. *J. Ethnopharmacol.* **2023**, *301*, 115833. [CrossRef] [PubMed]
16. Zhang, Q.; Yang, C.; Ma, S.; Guo, S.; Hu, X.; Zhou, Z.; Liu, Y.; Zhang, X.; Jiang, R.; Zhang, Z.; et al. Shiwei Qingwen Decoction Regulates TLR4/NF-κB Signaling Pathway and NLRP3 Inflammasome to Reduce Inflammatory Response in Lipopolysaccharide-Induced Acute Lung Injury. *J. Ethnopharmacol.* **2023**, *313*, 116615. [CrossRef] [PubMed]
17. Wang, S.; Lei, B.; Qi, L.; Guo, T.; Qi, Z.; Wu, S.; Yan, Z.; Gao, D.; Jiao, L.; Wang, J.; et al. Sanhuang Xiexin Decoction Ameliorates Acute Lung Injury by Disrupting NEK7-NLRP3 Inflammasome Activation. *J. Ethnopharmacol.* **2026**, *366*, 121624. [CrossRef] [PubMed]
18. Zeng, Z.; Fu, Y.; Li, M.; Shi, Y.; Ding, Q.; Chen, S. Guben Qingfei Decoction Attenuates LPS-Induced Acute Lung Injury by Modulating the TLR4/NF-κB and Keap1/Nrf2 Signaling Pathways. *J. Ethnopharmacol.* **2024**, *323*, 117674. [CrossRef] [PubMed]
19. Buchwald, W.; Szulc, M.; Baraniak, J.; Derebecka, N.; Kania-Dobrowolska, M.; Piasecka, A.; Bogacz, A.; Karasiewicz, M.; Bartkowiak-Wieczorek, J.; Kujawski, R.; et al. The Effect of Different Water Extracts from Platycodon Grandiflorum on Selected Factors Associated with Pathogenesis of Chronic Bronchitis in Rats. *Molecules* **2020**, *25*, 5020. [CrossRef]
20. Xie, L.; Zhao, Y.-X.; Zheng, Y.; Li, X.-F. The Pharmacology and Mechanisms of Platycodin D, an Active Triterpenoid Saponin from Platycodon Grandiflorus. *Front. Pharmacol.* **2023**, *14*, 1148853. [CrossRef] [PubMed]
21. Liu, Y.; Chen, Q.; Ren, R.; Zhang, Q.; Yan, G.; Yin, D.; Zhang, M.; Yang, Y. Platycodon Grandiflorus Polysaccharides Deeply Participate in the Anti-Chronic Bronchitis Effects of Platycodon Grandiflorus Decoction, a Representative of "the Lung and Intestine Are Related.". *Front. Pharmacol.* **2022**, *13*, 927384. [CrossRef] [PubMed]
22. Wang, L.; Wu, H.; Liu, C.; Jiang, T.; Yang, X.; Chen, X.; Tang, L.; Wang, Z. A Review of the Botany, Traditional Uses, Phytochemistry and Pharmacology of Stemonae Radix. *Phytochem. Rev.* **2022**, *21*, 835–862. [CrossRef]
23. Xiang, J.; Cheng, S.; Feng, T.; Wu, Y.; Xie, W.; Zhang, M.; Xu, X.; Zhang, C. Neotuberostemonine Attenuates Bleomycin-Induced Pulmonary Fibrosis by Suppressing the Recruitment and Activation of Macrophages. *Int. Immunopharmacol.* **2016**, *36*, 158–164. [CrossRef] [PubMed]
24. Kan, W.; Li, Q.; Li, P.; Ren, L.; Mu, W.; Lin, L.; Wen, J.; Ge, F.; Hou, M.; Hui, S.; et al. Glycyrrhiza Uralensis Polysaccharides Ameliorate Acute Lung Injury by Inhibiting the Activation of Multiple Inflammasomes. *J. Funct. Foods* **2023**, *100*, 105386. [CrossRef]
25. Wen, J.; Qin, S.; Li, Y.; Zhang, P.; Zhan, X.; Fang, M.; Shi, C.; Mu, W.; Kan, W.; Zhao, J.; et al. Flavonoids Derived from Licorice Suppress LPS-Induced Acute Lung Injury in Mice by Inhibiting the cGAS-STING Signaling Pathway. *Food Chem. Toxicol.* **2023**, *175*, 113732. [CrossRef] [PubMed]
26. Zhou, L.; Xiao, Y.; He, J.; Ren, H.; Zhao, C.; Zhang, C.; Shu, X.; Chen, Y.; Chen, D.; Chen, Y.; et al. Euchrenone A10 Attenuates Septic Lung Injury Though S100A8/A9-Dependent TLR4/MyD88/NF-κB Signaling. *Phytomedicine* **2025**, *148*, 157336. [CrossRef] [PubMed]
27. Wen, Y.; Ullah, H.; Ma, R.; Farooqui, N.A.; Li, J.; Alioui, Y.; Qiu, J. Anemarrhena Asphodeloides Bunge Polysaccharides Alleviate Lipoteichoic Acid-Induced Lung Inflammation and Modulate Gut Microbiota in Mice. *Heliyon* **2024**, *10*, e39390. [CrossRef] [PubMed]
28. Park, B.K.; So, K.S.; Ko, H.J.; Kim, H.J.; Kwon, K.S.; Kwon, Y.S.; Son, K.H.; Kwon, S.Y.; Kim, H.P. Therapeutic Potential of the Rhizomes of Anemarrhena Asphodeloides and Timosaponin A-III in an Animal Model of Lipopolysaccharide-Induced Lung Inflammation. *Biomol. Ther.* **2018**, *26*, 553–559. [CrossRef] [PubMed]
29. Kim, B.R.; Cho, Y.-C.; Le, H.T.T.; Vuong, H.L.; Lee, S.; Cho, S. Suppression of inflammation by the rhizome of Anemarrhena asphodeloides via regulation of nuclear factor-κB and p38 signal transduction pathways in macrophages. *Biomed. Rep.* **2017**, *6*, 691–697. [CrossRef] [PubMed]
30. Murray, P.J.; Allen, J.E.; Biswas, S.K.; Fisher, E.A.; Gilroy, D.W.; Goerdt, S.; Gordon, S.; Hamilton, J.A.; Ivashkiv, L.B.; Lawrence, T.; et al. Macrophage Activation and Polarization: Nomenclature and Experimental Guidelines. *Immunity* **2014**, *41*, 14–20. [CrossRef] [PubMed]
31. Wang, L.; Wang, D.; Zhang, T.; Ma, Y.; Tong, X.; Fan, H. The Role of Immunometabolism in Macrophage Polarization and Its Impact on Acute Lung Injury/Acute Respiratory Distress Syndrome. *Front. Immunol.* **2023**, *14*, 1117548. [CrossRef] [PubMed]
32. Zheng, J.; Li, Y.; Kong, X.; Guo, J. Exploring Immune-Related Pathogenesis in Lung Injury: Providing New Insights Into ALI/ARDS. *Biomed. Pharmacother.* **2024**, *175*, 116773. [CrossRef] [PubMed]

33. Yao, Q.; Wen, J.; Chen, S.; Wang, Y.; Wen, X.; Wang, X.; Li, C.; Zheng, C.; Li, J.; Ma, Z.; et al. Shuangdan Jiedu Decoction Improved LPS-Induced Acute Lung Injury by Regulating Both cGAS-STING Pathway and Inflammasome. *J. Ethnopharmacol.* **2025**, *336*, 118661. [CrossRef] [PubMed]
34. Yao, T.-T.; Zhang, Y.; He, R.-L.; Lv, X.; He, Y.-J.; Li, M.-Y.; Han, Y.-Y.; Long, L.-Z.; Jiang, G.-L.; Cheng, X.-Y.; et al. Mefunidone Ameliorates Lipopolysaccharide-Induced Acute Lung Injury through Inhibiting MAPK Signaling Pathway and Enhancing Nrf2 Pathway. *Int. Immunopharmacol.* **2022**, *113*, 109263. [CrossRef] [PubMed]
35. Guan, T.; Zhou, X.; Zhou, W.; Lin, H. Regulatory T Cell and Macrophage Crosstalk in Acute Lung Injury: Future Perspectives. *Cell Death Discov.* **2023**, *9*, 9. [CrossRef] [PubMed]
36. Zhang, L.; Gao, J.; Qin, C.; Liang, Y.; Chen, S.; Hei, F. Inflammatory Alveolar Macrophage-Derived Microvesicles Damage Lung Epithelial Cells and Induce Lung Injury. *Immunol. Lett.* **2022**, *241*, 23–34. [CrossRef] [PubMed]
37. Kellner, M.; Noonepalle, S.; Lu, Q.; Srivastava, A.; Zemskov, E.; Black, S.M. ROS Signaling in the Pathogenesis of Acute Lung Injury (ALI) and Acute Respiratory Distress Syndrome (ARDS). In *Pulmonary Vasculature Redox Signaling in Health and Disease*; Wang, Y.X., Ed.; Advances in Experimental Medicine and Biology; Springer International Publishing AG: Cham, Switzerland, 2017; Volume 967, pp. 105–137.
38. Millar, M.W.; Fazal, F.; Rahman, A. Therapeutic Targeting of NF-κB in Acute Lung Injury: A Double-Edged Sword. *Cells* **2022**, *11*, 3317. [CrossRef] [PubMed]
39. Ren, A.; Wang, H.; Zhu, H.; Ye, G.; Li, K.; Chen, D.; Zeng, T.; Li, H. Glycoproteins From Rabdosia Japonica Var. Glaucocalyx Regulate Macrophage Polarization and Alleviate Lipopolysaccharide-Induced Acute Lung Injury in Mice via TLR4/NF-κB Pathway. *Front. Pharmacol.* **2021**, *12*, 693298. [CrossRef] [PubMed]
40. Mantovani, A.; Dinarello, C.A.; Molgora, M.; Garlanda, C. Interleukin-1 and Related Cytokines in the Regulation of Inflammation and Immunity. *Immunity* **2019**, *50*, 778–795. [CrossRef] [PubMed]
41. Fields, J.K.; Guenther, S.; Sundberg, E.J. Structural Basis of IL-1 Family Cytokine Signaling. *Front. Immunol.* **2019**, *10*, 1412. [CrossRef] [PubMed]
42. Lei, Y.; Wang, K.; Deng, L.; Chen, Y.; Nice, E.C.; Huang, C. Redox Regulation of Inflammation: Old Elements, a New Story. *Med. Res. Rev.* **2015**, *35*, 306–340. [CrossRef] [PubMed]
43. Diao, Y.; Ding, Q.; Xu, G.; Li, Y.; Li, Z.; Zhu, H.; Zhu, W.; Wang, P.; Shi, Y. Qingfei Litan Decoction Against Acute Lung Injury/Acute Respiratory Distress Syndrome: The Potential Roles of Anti-Inflammatory and Anti-Oxidative Effects. *Front. Pharmacol.* **2022**, *13*, 857502. [CrossRef] [PubMed]
44. Li, H.; Feng, Y.; Sun, W.; Kong, Y.; Jia, L. Antioxidation, Anti-Inflammation and Anti-Fibrosis Effect of Phosphorylated Polysaccharides from Pleurotus Djamor Mycelia on Adenine-Induced Chronic Renal Failure Mice. *Int. J. Biol. Macromol.* **2021**, *170*, 652–663. [CrossRef] [PubMed]
45. Feng, W.; Han, X.; Hu, H.; Chang, M.; Ding, L.; Xiang, H.; Chen, Y.; Li, Y. 2D Vanadium Carbide MXenzyme to Alleviate ROS-Mediated Inflammatory and Neurodegenerative Diseases. *Nat. Commun.* **2021**, *12*, 2203. [CrossRef] [PubMed]
46. Yuan, H.; Wang, W.; Ma, J.; Li, H.; Reis, R.L.; Chen, Y.; Xu, X.; Yuan, Y.; Li, Y.; Yan, L.; et al. Inhalable PD-L1-Engineered Hybrid Cellular Vesicles Suppress Excessive Neutrophil Activation and Restore Mitochondrial Homeostasis to Alleviate Ischemia–Reperfusion Lung Injury and Pneumonia. *Bioact. Mater.* **2026**, *62*, 319–341. [CrossRef] [PubMed]
47. Tang, J.; Xu, L.; Zeng, Y.; Gong, F. Effect of Gut Microbiota on LPS-Induced Acute Lung Injury by Regulating the TLR4/NF-kB Signaling Pathway. *Int. Immunopharmacol.* **2021**, *91*, 107272. [CrossRef] [PubMed]
48. Mao, B.; Guo, W.; Tang, X.; Zhang, Q.; Yang, B.; Zhao, J.; Cui, S.; Zhang, H. Inosine Pretreatment Attenuates LPS-Induced Lung Injury through Regulating the TLR4/MyD88/NF-κB Signaling Pathway In Vivo. *Nutrients* **2022**, *14*, 2830. [CrossRef] [PubMed]
49. Chen, X.; Tang, J.; Shuai, W.; Meng, J.; Feng, J.; Han, Z. Macrophage Polarization and Its Role in the Pathogenesis of Acute Lung Injury/Acute Respiratory Distress Syndrome. *Inflamm. Res.* **2020**, *69*, 883–895. [CrossRef] [PubMed]
50. Liao, R.; Sun, Z.-C.; Wang, L.; Xian, C.; Lin, R.; Zhuo, G.; Wang, H.; Fang, Y.; Liu, Y.; Yang, R.; et al. Inhalable and Bioactive Lipid-Nanomedicine Based on Bergapten for Targeted Acute Lung Injury Therapy via Orchestrating Macrophage Polarization. *Bioact. Mater.* **2025**, *43*, 406–422. [CrossRef] [PubMed]
51. Laskin, D.L.; Malaviya, R.; Laskin, J.D. Role of Macrophages in Acute Lung Injury and Chronic Fibrosis Induced by Pulmonary Toxicants. *Toxicol. Sci.* **2019**, *168*, 287–301. [CrossRef] [PubMed]
52. Huang, X.; Xiu, H.; Zhang, S.; Zhang, G. The Role of Macrophages in the Pathogenesis of ALI/ARDS. *Mediat. Inflamm.* **2018**, *2018*, 1264913. [CrossRef] [PubMed]
53. Wang, J.; Li, R.; Peng, Z.; Zhou, W.; Hu, B.; Rao, X.; Yang, X.; Li, J. Gts-21 Reduces Inflammation in Acute Lung Injury by Regulating M1 Polarization and Function of Alveolar Macrophages. *Shock* **2019**, *51*, 389–400. [CrossRef] [PubMed]
54. Wang, L.; Yu, Q.; Xiao, J.; Chen, Q.; Fang, M.; Zhao, H. Cigarette Smoke Extract-Treated Mouse Airway Epithelial Cells-Derived Exosomal LncRNA MEG3 Promotes M1 Macrophage Polarization and Pyroptosis in Chronic Obstructive Pulmonary Disease by Upregulating TREM-1 via m6A Methylation. *Immune Netw.* **2024**, *24*, e3. [CrossRef] [PubMed]

55. Yan, S.; Xie, Y.; Xv, J.; Wang, K.; Wang, J.; Cao, Y.; Han, X.; Chen, F.; Zhou, L.; Jiang, Y.; et al. Shengjiang San Attenuates Sepsis-Induced Acute Intestinal Injury via *Lactobacillus Murinus* Derived IAAld-Mediated Macrophage Polarization through NF-κB and TGF-β Signaling. *J. Ethnopharmacol.* **2026**, *357*, 120910. [CrossRef] [PubMed]
56. Berman, A. Effects of Body Surface Area Estimates on Predicted Energy Requirements and Heat Stress. *J. Dairy Sci.* **2003**, *86*, 3605–3610. [CrossRef] [PubMed]
57. Reagan-Shaw, S.; Nihal, M.; Ahmad, N. Dose Translation from Animal to Human Studies Revisited. *FASEB J.* **2008**, *22*, 659–661. [CrossRef] [PubMed]

Disclaimer/Publisher's Note: The statements, opinions and data contained in all publications are solely those of the individual author(s) and contributor(s) and not of MDPI and/or the editor(s). MDPI and/or the editor(s) disclaim responsibility for any injury to people or property resulting from any ideas, methods, instructions or products referred to in the content.